

Review

Open Access



Recent progress in single atom catalysts for biomass conversion

Yuxin Gao^{1,#}, Jinling Cheng^{2,#}, Xiangwen Liu², Zhuohua Sun¹

¹State Key Laboratory of Efficient Production of Forest Resources, Beijing Forestry University, Beijing 100083, China.

²Institute of Analysis and Testing, Beijing Academy of Science and Technology (Beijing Center for Physical and Chemical Analysis), Beijing 100094, China.

[#]Authors contributed equally.

Correspondence to: Prof. Xiangwen Liu, Institute of Analysis and Testing, Beijing Academy of Science and Technology (Beijing Center for Physical and Chemical Analysis), Beike Building, No. 27, West 3rd Ring Road (North), Haidian District, Beijing 100094, China. E-mail: liuxiangwen@bcpc.a.ac.cn; Prof. Zhuohua Sun, State Key Laboratory of Efficient Production of Forest Resources, Beijing Forestry University, No.35 Qinghua East Road, Haidian District, Beijing 100083, China. E-mail: sunzhuohua@bjfu.edu.cn

How to cite this article: Gao, Y.; Cheng, J.; Liu, X.; Sun, Z. Recent progress in single atom catalysts for biomass conversion. *Microstructures* 2025, 5, 2025017. <https://dx.doi.org/10.20517/microstructures.2024.49>

Received: 31 May 2024 **First Decision:** 26 Jul 2024 **Revised:** 23 Aug 2024 **Accepted:** 30 Sep 2024 **Published:** 20 Feb 2025

Academic Editor: Liangzhi Kou **Copy Editor:** Ping Zhang **Production Editor:** Ping Zhang

Abstract

Biomass, as an emerging environmental and renewable resource derived from various green sources, is increasingly being recognized for its inherent structural characteristics that are conducive to the production of high-value chemicals. The complicated structure and oxygen-rich nature of biomass and its derivatives necessitate high-value targeted conversion, typically involving liquid-phase hydrogenation or the addition of acidic or basic environments. These processes impose stringent requirements on the efficiency and durability of the catalysts. Recently, the innovation of single atom catalysts (SACs) with individual catalytic sites dispersed on various supports has demonstrated high catalytic efficiency and good selectivity. Owing to their high atomic utilization and cost-efficiency, SACs have emerged as one of the most promising heterogeneous catalysts. This review summarizes current progress on the catalytic conversion of biomass mediated by SACs. Significant emphasis is placed on the unique active sites and reaction mechanisms of SACs in various kinds of catalytic methods (thermocatalysis, electrocatalysis, photocatalysis). In order to facilitate comparison, the various reactions are categorized according to the type of raw material (cellulose, hemicellulose, lignin, etc.). Especially, the developing strategies for preparing SACs are summarized to better satisfy industrial requirements. Finally, we provide an anticipatory outlook of future developments in this field, focusing on biomass utilization and advanced catalytic systems.

Keywords: Single atom catalysts, biomass, value-added products, selective catalysis



© The Author(s) 2025. **Open Access** This article is licensed under a Creative Commons Attribution 4.0 International License (<https://creativecommons.org/licenses/by/4.0/>), which permits unrestricted use, sharing, adaptation, distribution and reproduction in any medium or format, for any purpose, even commercially, as long as you give appropriate credit to the original author(s) and the source, provide a link to the Creative Commons license, and indicate if changes were made.



INTRODUCTION

Over the last decades, traditional fossil and coal energy have dominated as the primary energy sources in the global market. With the exhaustion of fossil fuels and escalating environmental pollution, it is particularly important to explore sustainable and environmentally friendly alternative energy sources. Biomass, one of the most abundant resources in the biosphere, is the only renewable carbon-based material and an ideal substitute for traditional fossil resources^[1,2]. It is postulated that the abundance of heteroatoms (such as oxygen) is linked to carbon atoms in biomass feedstocks. For fine chemicals and chemical intermediates, biomass energy is more suitable than fossil energy sources because of the abundance of C-O bonds, especially organic oxides. Therefore, the transformation of biomass resources into platform compounds for fuels and products, whether in a direct or indirect manner, offers a potentially lucrative value-added strategy.

Lignocellulose, a form of plant-derived biomass, makes up more than 90% of plant feedstocks and stands as the most plentiful carbon source that can be renewed^[3,4]. Lignocellulosic biomass, a functionalized biopolymer, mainly includes three macromolecules: cellulose, hemicellulose, and lignin with weight fractions of 40%-60%, 10%-40% and 15%-30%, and minor components such as starch, protein, and xylan^[5,6]. Cellulose, as the main component of lignocellulose, consists of up to 10,000 glucose units connected by β -glycosidic bonds with a high level of polymerization^[6-8]. The glucose derived from the hydrolysis of cellulose is an essential raw material for edible nutrition, pharmaceuticals and other industrial products^[9]. Hemicellulose is an amorphous polymer formed by C5 and C6 sugar units (including xylose, arabinose, mannose and galactose, among others) linked by β -glycosidic bonds^[6]. The structure of hemicellulose varies from plant to plant; for example, hardwoods consist mainly of xylose, whereas softwoods are composed mainly of mannose^[10]. The types of sugars that make up different raw hemicelluloses are varied. Cellulose and hemicellulose are general terms for the carbohydrates in lignocellulose, also called holocellulose. Lignin is a complicated group of phenolic polymers made up of three aromatic monomers: p-coumaryl alcohol, coniferyl alcohol, and sinapyl alcohol. The monomers are linked by unstable C-O bonds (e.g., β -O-4 and α -O-4) and resistant C-C bonds (e.g., β -5). The β -O-4 bond is a major bond form used to immobilize lignin-derived small molecules, which make up between 43% and 65% of native lignin, so the β -O-4 bond is usually easily broken during depolymerization. Lignin has potential as an alternative raw material for petroleum-based products due to its unique phenolic hydroxyl structure. These three components co-exist in the cell wall of the biomass feedstock and form a supramolecular network structure through complex interactions, which gives wood fiber excellent mechanical properties and resistance to physical, chemical and microbial degradation, but also leads to difficulties in biomass pre-treatment and components separation. The first step in the chemical catalysis process is to pretreat (e.g., ball milling, washing and consecutive acidic hydrolysis) raw lignocellulose into a range of platform small molecules (e.g., hexose, pentose, furans, guaiacol *etc.*). Then, these molecules are transformed into high-value chemicals through a series of reactions including hydrogenation, hydrodeoxygenation, oxidation, rearrangement, *etc.* Therefore, to optimally utilize each lignocellulosic component for the large-scale production of valuable biochemicals, chemical catalysis is regarded as the most promising method compared to thermochemical and biological transformations^[11-14].

Therefore, more efficient and durable catalysts are selected to increase the selectivity during the upgrading process. Similar to the catalyst selection for fossil feedstocks, heterogeneous catalysts have gained increasing popularity in the field of biomass utilization. Metals are considered as the core component of heterogeneous catalysts^[15], which were broadly used in the form of nanoparticles (NPs) during the past decades. The key advantage of metal NPs is the flexible parameters that can be adjusted to adapt to reaction requirements.

For example, the size of Ni particles presents considerable influence on the hydrodeoxygenation of m-cresol as the reducing Ni particle size from 9 nm to 1 nm, the direct deoxygenation rate increased by a factor of 10^[16]. Recently, Lim *et al.* applied a modular raspberry-colloid-templating technique to regulate the interparticle distance of PdAu alloy NPs; the result indicated a substantial increase in the selectivity of the hydrogenation of benzaldehyde as the distance increased from 12 to 21 nm^[17]. However, because of various factors, such as the dimensions of metal particles, carrier morphology, *etc.*, the regulation of catalytic parameters is a complex project. Meanwhile, only the surface atoms in NPs can be utilized, while the atom inside of the particle does not directly contribute to catalytic function, which greatly violates the principle of atom economy. Minimizing the size of NPs to a single atom provides the potential to solve the current problems.

In 2011, Zhang and his group successfully loaded single-atom Pt on FeO_x supports and presented the terminology of single atom catalysts (SACs) to define catalysis assisted by metal atoms^[18,19]. Compared to NPs or nanoclusters, SACs only have metal-support interaction instead of metal-metal interaction^[20]. Afterward, the new emerging SAC material exhibits significant advantages and potential in diverse catalytic domains such as energy conversion, environmental protection, organic synthesis, and electrochemical catalysis. The unique atomic-level dispersion and high catalytic efficiency of SACs enable them to address challenges in energy conversion, environmental protection, organic synthesis, and electrochemical catalysis. These advancements not only enhance our understanding of catalytic mechanisms but also pave the way for the development of more efficient and sustainable catalytic processes. The advancement of technology has led to the observation of evolving modes of existence for metal active sites on SACs. When the metal dispersion is 100% complete, it can be considered a single site. At this juncture, the carrier may be loaded with one or more metals. While the majority of studies have employed a single metal, there have been instances where three metal monoatoms have been loaded onto the same carrier, as documented in the literature^[21]. In some instances, metals are present on the same carrier as both single atoms and NP, which we consider to be dual-sites. These metals typically play different catalytic roles, facilitating more complex reactions. Additionally, alloy sites can be created through the loading of single atoms of one metal onto another. All three forms have been used in biomass catalysis. However, the primary challenge in preparing SACs lies in the precise manipulation of the geometric and electronic structures of the catalytically active metallic sites. Biomass feedstock has diverse functional groups (e.g., C=O, C=C, C-OH), adjusting the position (corner, edge, *etc.*) of individual metal atoms or the pore size of the support will alter the selectivity in the production of the target product. Furthermore, metal-ligand coordination dictates the adsorption of crucial intermediates, playing a vital role in the overall reaction process^[4]. Furthermore, the individual metallic atoms of SAC can be balanced on the support by diverse unsaturated chemical sites or spatial restriction, which not only maximizes the atomic economy, but also has the equity stability of a homogeneous catalyst.

Over the past decade, SACs have gained prominence across various fields, including thermal catalytic^[4,22-24], electrocatalytic^[25-27], and photocatalytic^[28] processes. A review of the literature shows that SACs are making great strides in processes such as carbon dioxide (CO₂) reduction^[29-32], O₂ reduction^[33,34] and the oxygen evolution reaction^[35,36]. Recently, with the renewed popularity of biomass resources, the field of biomass has witnessed the outstanding performance of SACs. In this context, much related work has been reported. Several review articles on this topic have been published recently. Mondelli *et al.* summarized the effect of metal-based solid catalysts on biomass transformation, with a concentration on the comparison of the reaction mechanism and catalytic impact of NPs and SACs^[15]. De *et al.* reviewed the recent research in biomass conversion of SACs, and all reports were categorized in the way of response types. Notably, the review concludes with insights into the design and application of SACs for industrial-scale biomass

conversion^[37]. Very recently, Chen *et al.* provided a comprehensive overview of the preparation and characterization of SACs, along with a detailed account of their catalytic applications in biomass conversion^[38].

This review offers a comprehensive overview on SACs employed in the chemocatalysis valorization of biomass, organized into three sections based on the type of catalysis (thermocatalytic, electrocatalytic and photocatalytic). Within each section, detailed discussions on platform molecules and reaction types are provided. The classification also highlights the distinct roles of various metal atoms in similar reactions and the interactions between different carriers and metals. Additionally, the review delves into the adsorption mode of catalysis and investigates the underlying reaction mechanisms. Recommendations are made for more efficient laboratory applications and large-scale industrial production. Finally, a vision and outlook for the current state of catalyzing the biomass landscape is presented.

THE APPLICATIONS OF SACS IN BIOMASS CONVERSION

Thermocatalysis

Over the past decades, a simple and primitive method of pyrolysis has been widely used for biomass resources. Biomass pyrolysis involves thermochemically converting biomass in an inert environment, typically established by introducing inert gases or creating a vacuum, under elevated temperature conditions, typically ranging from 400 °C to 550 °C^[39]. One of the main products of this process is bio-oil, which tends to have a complex composition and high oxygen content-disadvantages that hinder its further use. On this basis, catalysts have been introduced to overcome the problems of harsh reaction conditions and low selectivity of reaction products. In fact, thermal catalysis is the most widely used catalytic method in biomass conversion, and it is also the same in SACs. In this relatively mature approach to catalysis, research has increasingly focused on the design of structurally unique catalytic structures and the exploration of catalytic mechanisms. This sector will provide an all-inclusive overview of the role of SACs in biomass thermocatalysis, with a specific focus on classifying recent studies according to the nature of the reaction feedstock (cellulose, hemicellulose, lignin, *etc.*).

Cellulose and its derivatives

Compared to other biomass components, cellulose and its derivatives offer distinct advantages due to their simpler chemical structure and more accessible reaction properties, rendering them preferable for applications in the biorefinery industry. For example, the dehydration of fructose obtained through glucose isomerization can yield 5-hydroxymethylfurfural (HMF). In the utilization of cellulose, HMF and its subsequent derivatives are recognized as crucial and widely investigated platform molecules. This is due to their potential for transformation into a range of value-added chemicals through diverse pathways. As one of the three primary components, recent studies on SACs have centered on the conversion of small molecule compounds downstream of cellulose. Despite the efforts made to achieve the one-pot conversion of cellulose, the reactions involved present considerable challenges.

The conversion of HMF

HMF serves as a pivotal based compound in biomass utilization, acting as a connection between biomass resources, such as carbohydrates, and industrial products, including fossil fuels^[12]. This compound possesses highly reactive properties due to the existence of C=C, C=O, and furan ring chemical groups, which can be directly transformed into various economically valuable platform compounds [e.g., 2,5-dimethylfuran (DMF), 2,5-furandicarboxylic acid (FDCA), Levulinic acid (LA), *etc.*] through many reactions including hydrogenation, oxidation, and hydrodeoxygenation. In the selection of catalysts, a shift from noble metals

NPs to SACs has been experienced in order to overcome disadvantages such as low selectivity, harsh reaction conditions and complicated separation^[15,39]. For instance, in 2017, non-noble Ni-Co/C catalyst achieved high yield conversion in HMF hydrogenolysis^[40]. The following year, supported Pt-Co bimetallic NPs achieved a high yield of DMF (> 90%) under moderate conditions in the same reaction^[41]. Nonetheless, the previously mentioned catalysts exhibit several drawbacks, including high noble metal loadings, inefficient utilization of noble metal atoms, and a scarcity of exposed active sites^[42]. As a result, scientists have started to search for a balance between atomic utilization and catalytic efficiency.

In recent years, researchers have reduced the scale of metal particles to single atoms, as compared to their relevant NP-based catalyst systems. For example, the hydrodeoxygenation of HMF can be converted to DMF and other derivatives such as HMF, 5-methylfurfural (MF), 2,5-dihydroxymethylfuran (DHMF), DMF, 5-methylfurfuryl alcohol (MFA), *etc.*, as shown in [Scheme 1](#). It should be noted that DMF generated from the hydrodeoxygenation of HMF is a key precursor to yield sustainable liquid fuels. In 2020, Gan *et al.* introduced a simple, environmentally friendly, and scalable ball milling technique for synthesizing Co-alloyed Pt single-atom alloy (SAA) catalysts. Catalyst preparation applies acetylacetone as a precursor and a scalable ball milling method for synthesis, leading to the production of SAA on a kilogram scale [[Figure 1A](#)]. These catalysts demonstrated exceptional catalytic efficiency in the hydrodeoxygenation of HMF, achieving 92.9% selectivity to DMF. Parallel experiments evaluated the catalytic efficiency of Co nanocrystal catalysts (without Pt doping) and Pt₁/Co SAA by analyzing reaction time and selectivity and hypothesized the reaction pathway of HMF [[Figure 1B](#)]^[42]. The result shows that, HMF was completely transformed into Pt₁/Co catalysts at a very short time, but the selectivity of individual intermediates is so low. When the reaction time was extended to 120 minutes, 92.9% of DMF was obtained, while HMF conversion remained nearly constant at 100%. Concurrently, the primary intermediates, DHMF and MFA, were almost fully converted. As depicted in [Figure 1C](#), it is hypothesized that the C=O bond in HMF is initially hydrogenated, leading to the formation of DHMF intermediates. Subsequently, the dehydroxylation process, less hindered by the barrier of furan ring opening compared to CH₂-OH bond cleavage, resulted in the production of DMF. The catalyst maintains a good hydrodeoxygenation efficiency after five cycles and because of the magnetic properties of Co, the catalyst can be separated by an external magnetic force. In 2021, a robust SAC with double reactive sites was reported, consisting of atomic Pt on an intermetallic Ni₃Fe substrate (Pt₁/Ni₃Fe IMC). This catalyst achieved high catalytic efficiency with almost complete conversion of HMF in 30 minutes and a high yield of DMF in 90 minutes. Reasonably controlled experiments and first-principles calculations confirmed that Pt₁/Ni₃Fe IMC facilitated a two-step hydrodeoxygenation via an interfacial tandem catalytic mechanism: firstly, the hydroconversion of HMF to DHMF, and secondly, the hydrodecomposition of DHMF to DMF. In this process, the single Pt site is responsible for the hydrogenation of the C-O group, while the Ni₃Fe interface promotes the cleavage of the C-OH bond^[43]. At the same time, a single-atom Pt (0.4 wt%) anchored on Co₂AlO₄ spinel support is also utilized in HMF conversion; the final DMF yield generated is up to 99% and the turnover frequency (TOF) is 2,553 h⁻¹, achieving the peak performance reported among heterogeneous catalysts. Single platinum atoms are loaded on the surface of Co₂AlO₄ by bonding with surface oxygen atoms, creating a synergy between the platinum atom sites and the adjacent Brønsted acid sites^[44].

Transfer hydrogenation (TH) of HMF is also a visionary study, one of the challenges being that the C=O bond is easier to break than the C-OH bond. In 2021, Li *et al.* reported the highly selective generation of MF using hydrogen as a reducing agent. They chose oxygen defective Nb₂O₅ as the carrier and loaded single metal atoms (Pt₁, Pd₁, Au₁) onto the it. It was found the interaction of the Pt and Nb sites at the catalyst interface, where the metal and the carrier are in contact with each other. Responsible for H₂ activation, Pt₁/Nb₂O₅-Ov is very active for the catalysis of the C-OH bond, allowing the MF to obtain close to full

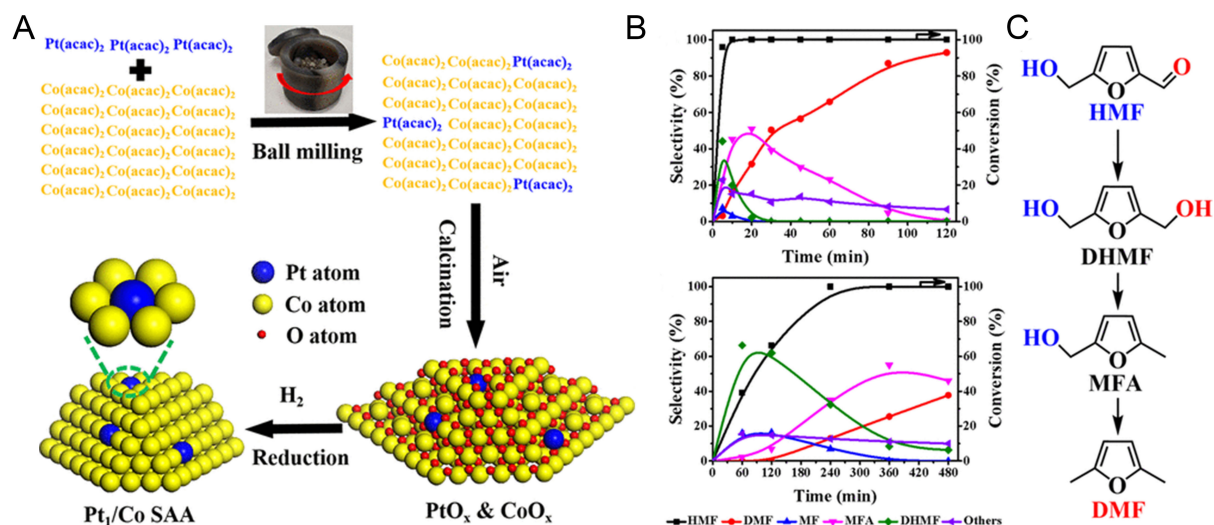
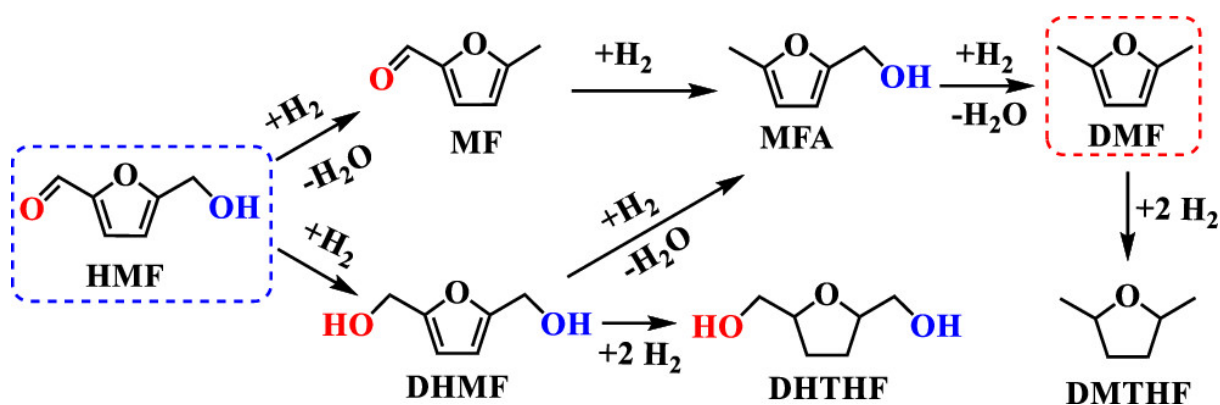


Figure 1. (A) Schematic illustration of preparation of Pt₁/Co SAA catalysts using ball milling; (B) Product distribution of the HMF hydrogenolysis as a function of reaction time over (up) Pt₁/Co SAA and (down) Co nanocrystals catalysts; (C) Main route for the hydrogenolysis of HMF to DMF^[42]. Copyright 2020 American Chemical Society. SAA: Single-atom alloy; HMF: 5-hydroxymethylfurfural; DMF: 2,5-dimethylfuran.



Scheme 1. Hydrodeoxygenation of HMF to DMF and other byproducts^[42]. Copyright 2020 American Chemical Society. HMF: 5-hydroxymethylfurfural; DMF: 2,5-dimethylfuran.

selectivity^[45].

Oxidation products, FDCA and 2,5-diformylfuran (DFF) of HMF, are precursors for the polymer industry and byproducts in the transformation of lipid acids to biodiesel, transforming them into upgrades products. Afterwards, there are examples reported of a Co-based double-site catalyst. 5-hydroxymethyl furfural oxidation reaction (HMFOR) is a tandem reaction that proceeds in two steps: the transformation of an aldehyde into a carboxylic acid and the intermediate conversion of a hydroxyl group into an aldehyde. A single active site showed different activities in the two oxidation reactions, resulting in suboptimal catalytic performance for converting HMF to FDCA. Hence, composite catalysts with dual active sites could offer a promising solution for complex tandem catalysis. Transmission electron microscopy (TEM) exposed that annealing resulted in the formation of numerous Co-loaded carbon nanotubes (CNTs) on the surface of N-doped carbon rhombic dodecahedra [Figure 2A]. In addition, cobalt NPs are produced by reduction of volatile gases from the decomposition of organic linkers, which are confined to the tips of CNTs or are

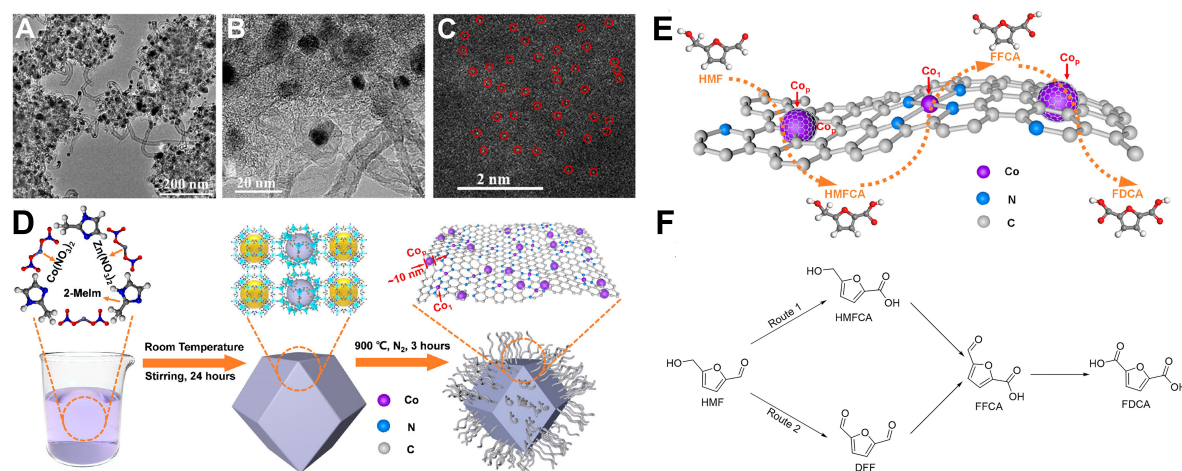


Figure 2. (A, B) TEM images of (Co₁→Co_p)/N-CNTs; (C) HAADF-STEM image of (Co₁→Co_p)/N-CNTs in the nanoparticle free region, where single Co atoms are clearly seen; (D) Schematic Illustration for the Synthesis of (Co₁→Co_p)/N-CNTs from ZnCo-ZIF; (E) Schematic Illustration of HMF Conversion to FDCA Accelerated by Different Reactive Sites (Co₁ and Co_p); (F) Reaction Routes for the Aerobic Oxidation of HMF to FDCA^[46]. Copyright 2022 American Chemical Society. TEM: Transmission electron microscopy; CNTs: carbon nanotubes; HAADF-STEM: high-angle annular dark-field scanning TEM; HMF: 5-hydroxymethylfurfural; FDCA: 2,5-furandicarboxylic acid.

encapsulated in CNTs [Figure 2B]. Particularly, as demonstrated in Figure 2C, multiple bright dots on the carbon framework in regions free of metal particles indicated the presence of individual Co atoms. Co atoms and NPs work synergistically, enabling the catalyst to efficiently oxidize hydroxyl groups to aldehydes and aldehydes to carboxyl groups. This catalyst comprises rhombic dodecahedral ZnCo-ZIF, exposed to controlled pyrolysis at 900 °C under a N₂ atmosphere [Figure 2D]. This cooperation enhances performance in the oxidation of HMF to FDCA [Figure 2E]^[46]. Furthermore, a kind of Mn-Co dual-single-atom catalyst demonstrates a unique synergy in enhancing O₂ activation through the cooperation of two different activation processes. It exhibited excellent catalytic properties for oxidative-driven esterification of HMF. In contrast to the previous dual active site catalytic mechanism, the coexistence of two types of reactive oxygen species (ROS) effectively facilitates the oxidation of hydroxyl and aldehyde groups^[47]. Figure 2F is a diagram of the two pathways of HMF oxidation.

Meanwhile, a type of research uses the downstream products of HMF as the substrate. The earliest study was that in 2016, Zhang *et al.* first reported γ -AlOOH nanosheets with dispersed Pd species on them. Even with a very low Pd loading, 0.1Pd/ γ -AlOOH exhibits a catalytic activity that achieves 50.3% succinic acid conversion in 4 hours^[48]. Very recently, Liu *et al.* reported a fabricate a highly polar Pd-N₃ site through the special Pd-based catalysts (Pd₁/BNC). Combining single metal atoms with highly polarized boron nitrogen doped carbon (BNC) carriers and creating new atomically linked active centers is a new supramolecular controlled pyrolysis strategy. This Pd₁/BNC catalyst enables the full-spectrum amination of biomass-derived aldehydes/ketones, a green and environmentally friendly way of producing aromatic and furanic amines^[49]. The hydrogenation of biomass maleic anhydride (MAH) has been studied relatively infrequently. In August of 2023, Sun *et al.* anchored Pt single atoms to Mo vacancies at the edge of specific 1T-phase MoS₂ creating a unique pocket of active sites. This Pt₁/1T-MoS₂ SAC could adjust the adsorption and hydrogen dissociation, showing a complete selectivity of MAH to succinic anhydride under mild conditions^[50].

The conversation of LA

LA is a crucial intermediate platform compound of biomass that can be produced through the conversation of HMF under acidic conditions. Recently, there has been significant research concentrated on the catalytic conversion of LA using various catalysts. LA hydrotreating to γ -valerolactone (GVL) has always been the subject of much enthusiasm, due to its great potential for high-density fuels and biobased polymers. In 2021, Han *et al.* reported about the hydrogenating LA to GVL in solvent-free conditions^[51]. The catalyst was synthesized using notched-polyoxometalate (N-POM) to connect Ru atoms and prevent Ru from aggregating during pyrolysis. As demonstrated in [Figure 3A](#), SiO₂ was used as a template and an anion exchange strategy was used to move POM-containing Ru ions into a pre-synthesized anionic polymer covered with SiO₂. Pyrolysis, followed by etching to remove the SiO₂ template, yielded the Ru₁@WO_x/CN catalyst. Some related commercial catalysts such as the Ru₁/CN catalyst, commercial Ru/C, and Ru₁@WO₃ were also prepared and explored for comparison [[Figure 3B](#)]. The Ru₁@WO_x/CN catalyst exhibits an outstanding catalytic performance (almost complete conversion and selectivity). In turn, a case reported a range of Ru-Co SAA catalysts. It efficiently hydrogenates LA under aqueous phase conditions, evaluated to the presence of better electron-abundant Ru atoms. Ru, at the atomic level, enhances LA/H₂ adsorption, H₂ dissociation and C=O hydrogenation in LA by lowering the reaction energy barriers compared to the same pure metal^[52].

In June 2022, Gao *et al.* proposed a reaction method for the targeted reductive amination of LA and related keto acids. This atomically dispersed cobalt-based SAC catalyst exhibits remarkable activity and excellent substrate breadth compared to its Co NP counterpart. Various isoindolinones were synthesized from aromatic keto acids and amine/nitro compounds using the optimal catalyst system [[Figure 3C](#)]^[53].

One-pot conversion of cellulose

A highly attractive approach for cellulose is its straightforward conversion into valuable molecules. In 2008, before the SAC concept was born, Doc. Zhang and his group reported that a small amount of nickel could promote the carbon supported tungsten carbide (W₂C/AC) catalyst system for cellulose conversion into polyols, especially ethylene glycol and sorbitol^[54]. Later, the same group reported a Pt-Cu/SiO₂ SAA catalyst, for ethanol production from cellulose. Platinum NPs avoid the C-C bond cleavage side-reaction that is usually induced by the native form of platinum. Consequently, methyl glycolate can be converted into ethanol at lower temperatures, significantly enhancing ethanol selectivity^[55]. Ordinary SACs usually face problems such as atomic aggregation, high-temperature intolerance, *etc.* Ni metal is unstable under acidic conditions, but the hydrogenation process inevitably encounters acidic conditions. To solve those problems, Liu *et al.* developed a stable Ni-N-C SAC with an actual metal use content of 7.5 wt%. The catalyst exhibited outstanding catalytic activity and durability for the one-pot conversion of cellulose under extremely harsh conditions (245 °C, 60 bar H₂, presence of tungstic acid in hot water). Extensive spectroscopic characterization and computational modeling revealed that (Ni-N₄)-N is the active center of the catalyst and that covalent bonding between N and Ni atoms is responsible for maintaining the stability of this catalyst^[56]. Recently, Zhang *et al.* designed a catalyst composed of Ru single atoms and Ru NPs on a carbonized melamine foam (CMF) support [[Figure 4A](#)]. The mixed LA and HMF substrates were efficiently converted to the desired products of GVL and FDCA without any purification steps. This efficiency is attributed to the distinct advantages of the single-atom and NP sites. In high-angle annular dark-field scanning TEM and electron microscopy, it was demonstrated that Ru metal exists on the carrier in two forms [[Figure 4B-E](#)]. They showed the cooperative mechanism in [Figure 4F](#), the metallicity of Ru-SA is reduced compared to Ru-NP, thus inhibiting reactant adsorption. So, multiple active sites in Ru-NP have good adsorption capacity for reactants and intermediates, and the presence of Ru-SA helps a lot in the hydrogenation of LA. In summary, Ru-single atoms triggered LA while Ru-NPs enhanced hydrogen dissociation, promoting the

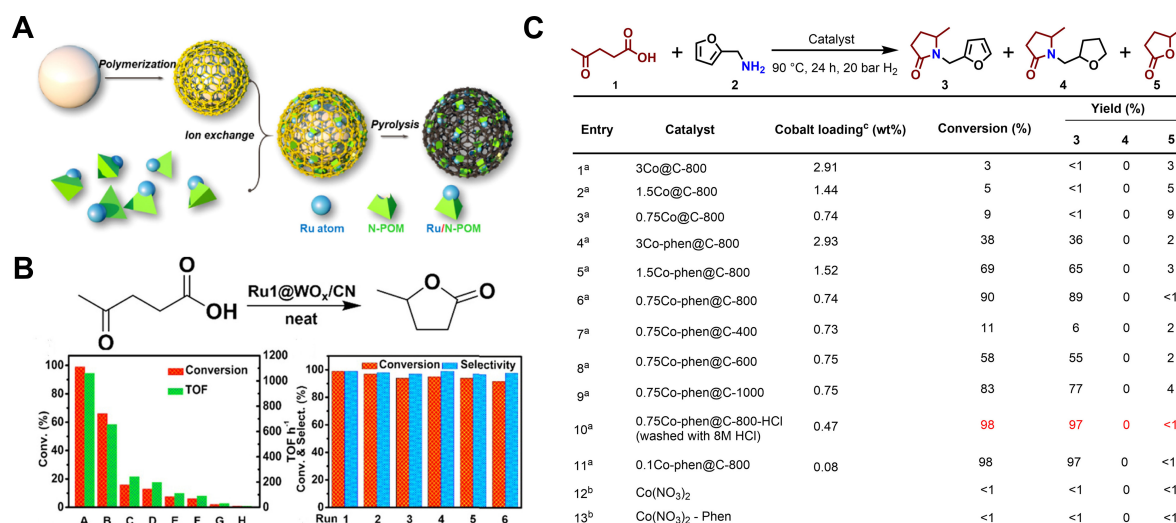


Figure 3. (A) Schematic illustration of the synthesis of Ru₁@WO_x/CN; (B) The conversion (%) and the overall turnover frequency of LA to GVL for the Ru₁@WO_x/CN (Label A in the figure), and other commercial catalysts (left). The recycling text of the Ru₁@WO_x/CN catalyst^[51]. Copyright 2021 American Chemical Society; (C) Screening of different catalysts for LA reductive amination^[53]. Copyright 2022 Elsevier. LA: Levulinic acid; GVL: γ -valerolactone.

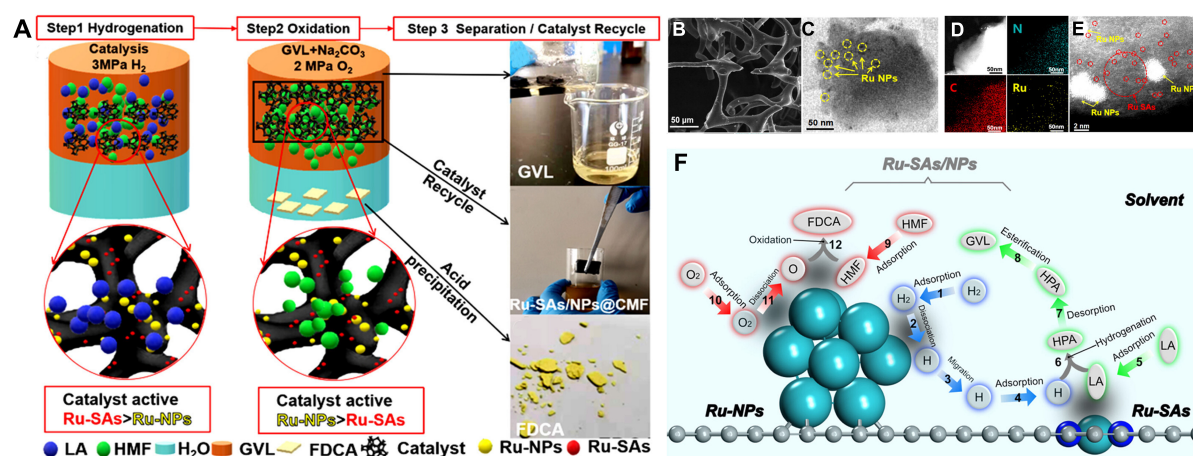


Figure 4. (A) Schematic of the catalytic alternate hydrogenation-oxidation process; (B) Scanning electron microscopy and (C) transmission electron microscopy images of the catalyst containing only Ru nanoparticles; (D) Elemental distribution mappings; (E) high-angle annular dark-field scanning transmission electron microscopy images^[57]. Copyright 2023 American Chemical Society.

hydrogenation reaction and ensuring the productive conversion of HMF to FDCA through oxidation. The biphasic solvent system enhanced mass transfer and enabled spontaneous, energy-efficient separation of the resulting products: GVL and FDCA^[57].

Hemicellulose and its derivatives

Furfural is an important downstream compound of hemicellulose, which is produced by hydrolysis of hemicellulose from lignocellulosic biomass catalyzed by dilute acids. This compound is the most significant derivative of the furan ring system, exhibiting chemical reactivity, capable of undergoing oxidation, condensation, and other reactions to generate a multitude of derivatives. It is a prevalent component in synthetic plastics, pharmaceuticals, pesticides, and other industrial applications. Therefore, the current

application of SACs in hemicellulose also focuses on various transformations of furfural.

The conversation of furfural

Furfural contains furan rings, cyclic ether bonds and carbonyl groups that are highly reactive, which can be converted into many synthetic chemicals such as furfuryl alcohol (FAL), tetrahydrofurfuryl alcohol (THFA), 2-methylfuran (2-MF), cyclopentanone, and furan by hydrogenation, hydrogenation-hydrolysis and decarbonylation.

For example, Pd nanoclusters on zirconia (ZrO_2) and single Pd atoms on ceria (CeO_2) displayed great catalytic activity for the decarbonylation of furfural to furan in the liquid phase without any additives. Fu *et al.* investigated the active size of Pd and the alterations in chemical states occurring throughout the reaction. It has been observed that individual Pd atoms exhibit positive characteristics, whereas clusters of Pd are effective in promoting decarbonylation. The lower binding and migration energies of Pd_1/ZrO_2 indicate that palladium atoms are able to diffuse across the ZrO_2 surface, leading to the formation of small palladium clusters. Conversely, Pd atoms on CeO_2 exhibit a reduced tendency to diffuse and instead tend to aggregate at stable sites, resulting in the formation of larger palladium NPs. It was concluded that ZrO_2 is the most suitable support for steadying Pd clusters, as it exhibits better catalytic properties during the reaction^[58,59]. Metal-support interactions are a classical problem explored in multiphase catalytic systems. This study uses titanium dioxide or mesoporous graphitic carbon nitride as carriers to explore the role played by Ir metal monoatoms on different carriers^[60]. Later, another research demonstrated a method to selectively cleave the C-O bond using furfuryl alcohol conversion to 2-MF as a showcase. When surface-doped with an ultralow loading of Pt (comprising single atoms and sub-nanometer clusters), the material demonstrates an activity nearly two orders of magnitude higher than that of pure TiO_2 . Figure 5A shows that this ultra-low loading SAC can effectively improve the selectivity over the previous multi-site catalysts. According to the reverse Marsvan Krevelen mechanism, metal oxides are considered one of the most promising classes of catalysts for C-O bond cleavage, but the most active oxides experience bulk reduction during the reaction. Density functional theory (DFT) and microkinetic calculations show that this catalytic mechanism generates a catalytic cycle. In this cycle, molecular hydrogen facilitates vacancy formation, followed by FA adsorption, C-O bond cleavage with hydrogen back-donation from the departing OH to carbon, and finally, 2-MF desorption [Figure 5B]. The metal atom directly bonded to the interfacial oxide is the most active center in the tandem reaction^[58]. On layered double oxides [Mg(Al)O] containing magnesium and aluminum, platinum atoms exist as dispersed monoatoms, coordination-unsaturated two-dimensional (2D) clusters and three-dimensional clusters. Directed activation of C-OH, C-O-C or C=C was investigated. These three types of platinum sites were used for the hydrogen conversion of FAL to 2-MF, THFA or 1,2-PeD, respectively [Scheme 2]^[61].

Interestingly, lowering the concentration of Ru on the support enhances the catalyst system's activity. This behavior is attributed to the unique $\text{Ru}_1\text{Co}_{\text{NP}}$ surface SAA structure, which is only allowed at high Co/Ru ratios ($\text{Co/Ru} \geq 10$) on the hydroxyapatite support^[62]. Notably, non-precious metals are very attractive for SAC applications. To create different Fe sites, enabling them to be preferentially utilized in activating C-O bonds selectively. An *et al.* used $\text{Fe}(\text{NO}_3)_3$ as an iron source for saturable adsorption and pyrolysis on a ZIF-8 substrate to form SAC at ultra-low Fe contents (< 0.1 wt%) [Figure 6A]^[63]. X-ray absorption near-edge structure (XANES) and Fourier transforms (FTs) of EXAFS spectra prove that Fe and Zn in Fe-ZIF-800 have lost their metallicity and are instead coordinated to O/N [Figure 6C]. Their performance exceeds other Fe catalysts by up to four orders of magnitude, achieving a great yield of FA and almost complete conversion of furfural in just one hour [Figure 6D]. The flexible coordination structure of the $\text{Fe}(\text{II})\text{-p}_1\text{N}_3$

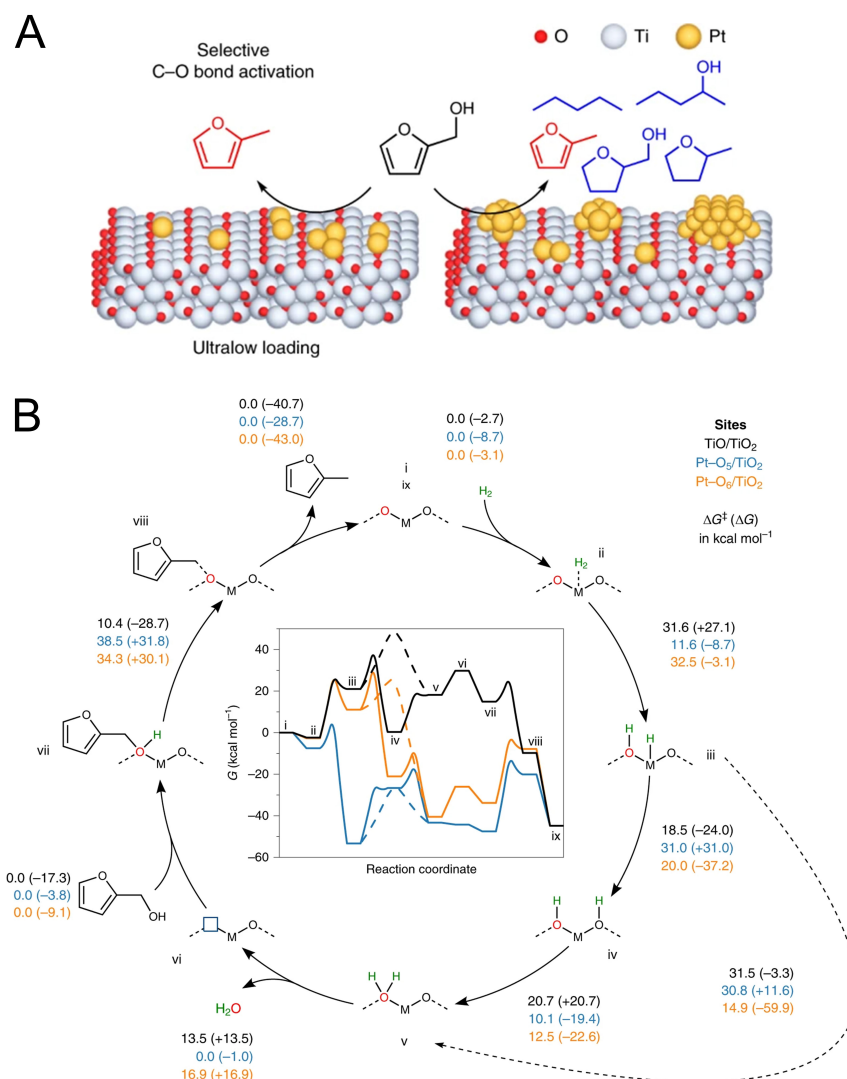


Figure 5. (A) Reactions of furfural with different catalysts; (B) Catalytic cycle for FA upgrade on (101) TiO₂ anatase surface. Numbers and free energy profiles represent pure TiO₂ (black), Pt-O₂/TiO₂ (blue) and Pt-O₆/TiO₂ (orange). DFT-based Gibbs barriers, ΔG^\ddagger , (reaction energies, ΔG) in kcal mol⁻¹. Gibbs energies are reported with respect to the energy of the pristine surface and H₂ and FA chemical potentials, computed at experimental conditions (Methods)^[58]. Copyright 2020 Nature Publishing Group. DFT: Density functional theory; FA: furfuryl alcohol.

active center in Fe-ZIF-800 allows for the co-adsorption of the furfuryloxy and hydroxyl groups, which reduces the stress on the iron atoms to some extent. Isotopic labeling experiments have demonstrated that the catalytic transfer hydrogenation (CTH) reaction proceeds via intermolecular hydride transfer, adhering to the Meerwein-Ponndorf-Verley (MPV) mechanism, instead of metal-mediated hydrogenation [Figure 6B]. Staff tested the catalyst on the same type of ketone substrate, demonstrating its universality.

Lignin and its model compounds

Lignin, a crucial constituent of lignocellulosic materials, represents one of the three primary components. It manifests as a 3D non-crystalline polymer, characterized by methoxylated phenylpropane structures. Due to its significant amount of aromatic structure and higher carbon and lower oxygen content, lignin has been generally recognized as a viable alternative to petroleum. However, it remains the least utilized

effective in both hydrogenation and hydrodeoxygenation of vanillin in water [Figure 7A]^[70]. At 60 °C, only vanillyl alcohol is formed. As the temperature increases, further hydrogenation occurs to produce a mixture of vanillyl alcohol and 2-methoxy-*p*-cresol. At 140 °C, only 2-methoxy-*p*-cresol is formed. This provides an excellent illustration of the catalytic mechanism of SACs at varying temperatures. The catalyst can achieve 100% conversion within 15 min, with conversion and TOF far exceeding those of comparable commercial catalysts. Also, it is noteworthy that the catalyst maintains a very good catalytic effect after ten cycles [Figure 7B]. They proposed a systematic reaction mechanism using first-principles calculations, indicating that the barrier to vanillin hydrogenation is too high and only vanillin is formed. When the temperature rises, there are two transition states (IM2, IM3) after the adsorbed phase of vanillyl alcohol, making it possible for further deoxygenation of vanillyl alcohol to MMP (4-hydroxy-3-methylaniso) [Figure 7C]. Therefore, vanillyl alcohol is the product that prohibits deoxygenation, while 2-methoxy-*p*-cresol is the product that allows deoxygenation. To prevent the metal species from being reduced and forming nanoclusters when using WO_{2.72} (violet tungsten oxide) as a support, a one-step in situ synthesis method was developed to create dispersed metal atoms. Dispersed palladium atoms on WO are covalently bonded to oxygen atoms in the vicinity of the support to form an active center. Besides efficiently catalyzing vanillin, under optimized conditions, most lignin-derived species (such as *o*-vanillin, syringaldehyde, isovanillin, ethylvanillin, and 4-hydroxybenzaldehyde) can be effectively and selectively transformed into their respective products^[71].

Benzyl alcohol

Benzyl alcohol (BA) is regarded as a model compound for lignin-derived alcohols. The following examples will examine SACs using BA oxidation as the probe reaction. In 2017, bimetallic Au@Pd/TiO₂ catalysts were prepared. Pd atoms were deposited on the bare surface of gold NPs to form core-shell mixed metal particles with simultaneous electron transfer between the cores. The Pd species dominated the aerobic oxidation of BA without solvents. The BA conversion grew with palladium deposition at low palladium deposition levels, but remained constant when the palladium deposition was further increased to 0.13 wt%^[72]. Subsequently, Li *et al.* prepared a series of SACs by adsorbing different metals (Pt, Au) on CeO₂, which were tested using BA oxidation as a model reaction. Compared to the corresponding NP catalysts, SACs have the maximum number of interfacial sites, resulting in a much higher activity^[73]. This configuration enables this efficient and sustainable hydrogenation reaction to occur exclusively in aqueous solution. In 2019, influenced by natural iron-catechol complexes in marine mussels, Zhou *et al.* synthesized metal-lignin coordination complexes with different metals on nitrogen-doped carbon to generate SACs. They proposed a full lignocellulose utilization strategy where oxygenates derived from lignin are transformed into valuable building blocks and fragrances using a Co SAs-N@C catalyst [Figure 8]^[74].

Anisole

Eco-friendly conversion of biomass-sourced molecules into cyclohexanone, a feedstock for nylon preparation, is highly sought after. In this context, a Pd SAC anchored in the micropores of zeolite (Pd₁/ZSM-5) is designed to solve this problem. This catalyst demonstrated potential for the hydrogenation of anisole to cyclohexanone of initial hydrogen pressure, achieving a cyclohexanone selectivity of 91.2 ± 1.8%. Additionally, water is not only directly involved in this reaction but also acts as a green solvent, adsorbing and activating anisole to form the green water addition-elimination mechanism^[75].

Depolymerization of lignin

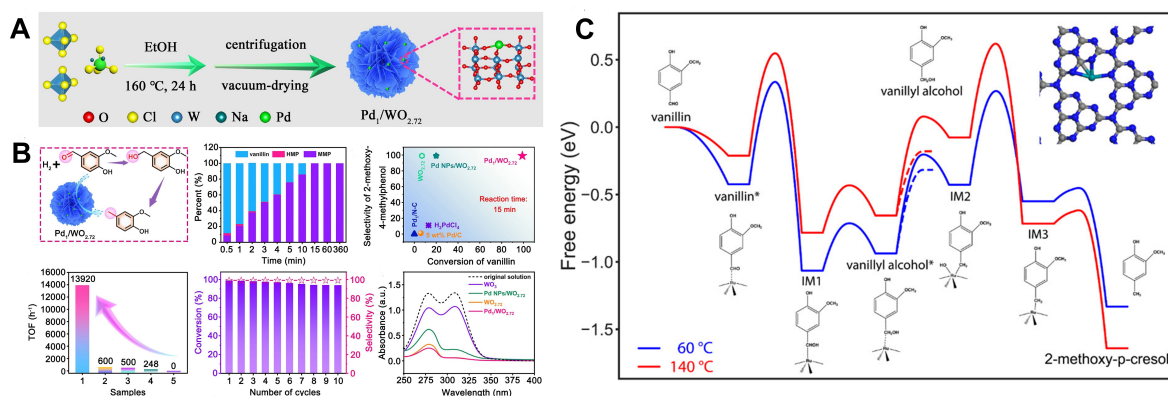


Figure 7. (A) Synthetic route for the construction of Pd₁/WO_{2.72}; (B) Catalytic performance of Pd₁/WO_{2.72}. Including conversion and selectivity, performance comparison with other similar catalysts, TOF values and recycling performance; (C) Free energy diagrams of vanillin hydrogenation to vanillyl alcohol and 2-methoxy-2-methoxy-p-cresol at 60 °C (blue) and 140 °C (red). The structures of reactants and products are shown above the energy profiles, while the intermediate state structures are shown below the energy profiles. The geometry of Ru₁/mpg-C₃N₄ is shown in the upper right^[70]. Copyright 2018 American Chemical Society. TOF: The turnover frequency.

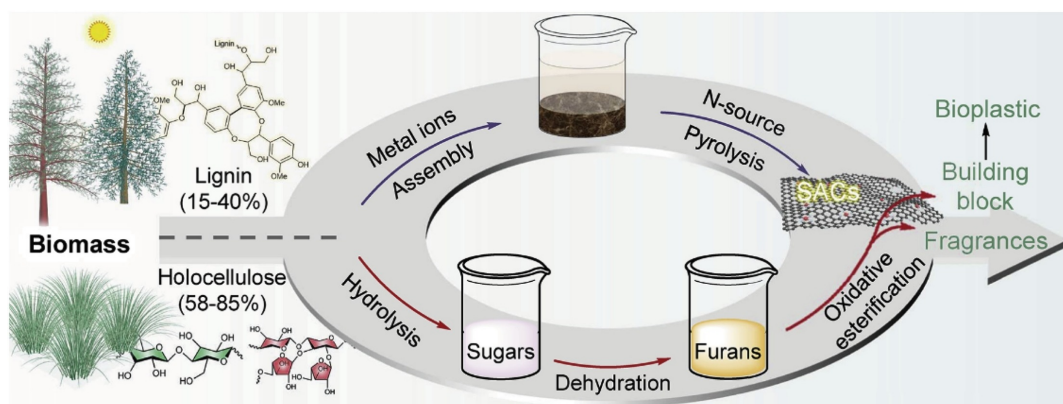
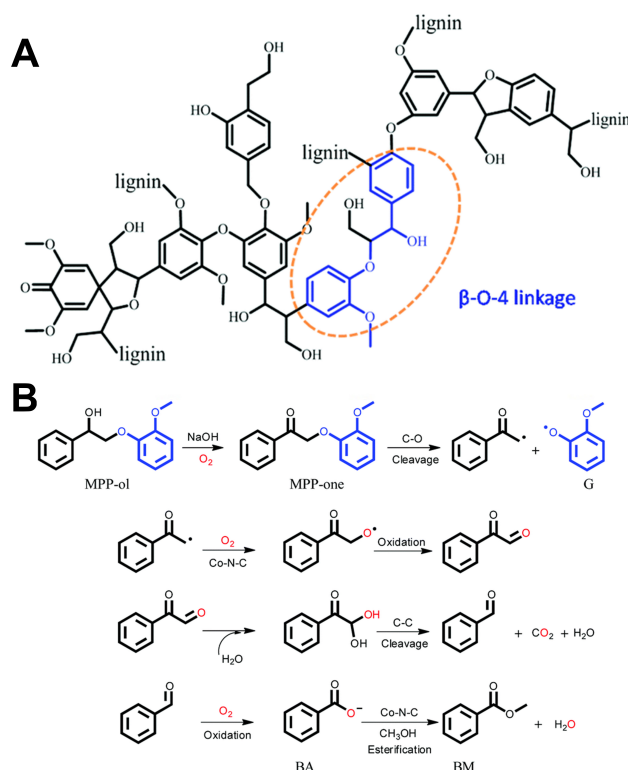


Figure 8. Engineering metal-lignin (M-L) complexes to SACs for the upgrading of carbohydrate-derived furans^[74]. Copyright 2019 Elsevier. SACs: Single atom catalysts.

Lignin's polymerized structure is very sturdy due to its structural units of phenylalanine which connect by C-O and C-C linkages. Thus, some researchers try to use lignin-derived dimer/special linkages structural model compounds instead of real lignin to investigate the catalytic mechanisms involved. The β -O-4 bond is the most common connecting bond in lignin and is more easily broken than the C-C bond in the lignin structure [Scheme 3A]. Therefore, some research starts from "friendly" β -O-4 linkage to open the structure of lignin. For example, atomic Co catalyst (Co-N-C) is applied for the oxidative cleavage of 2-(2-methoxyphenoxy)-1-phenylethanol (MPP-ol). In the presence of O₂ and NaOH, MPP-ol is converted to MPP-one first. The C-C bond in phenylacetaldehyde breaks to form BA, which then reacts with methanol (MeOH) to form BM [Scheme 3B]^[76]. The hydroxyl group in Ca was oxidized, weakening the β -O-4 bond, and the yield of MPP-ol was increased to 95% under mild conditions (150 °C, 4 h). This also demonstrates the promise of SACs for β -O-4 bond breaking applications.

Guaiacol and its derivatives



Scheme 3. (A) Representative structure of a lignin fragment with the β -O-4 linkage; (B) Proposed reaction pathway of MPP-ol^[76]. Copyright 2019 Elsevier. MPP-ol: 2-(2-methoxyphenoxy)-1-phenylethanol.

Lignin can be depolymerized through reduction or thermal treatment to produce bio-oil. Bio-oil is mainly composed of lilac-based and guaiac-based compounds, which contains many phenolic monomers functionalized with an alkyl group at the para position and methoxy group at the ortho positions. Hydrodeoxygenation of lignin oil (LO) produces high-value fuels. The aromatic and olefin structures in bio-oils are not saturated enough; hydrodeoxygenation can help them reduce the oxygen percentage and raise the calorific value of bio-oils through a higher H/C ratio. During this process, we expected selective cleavage of C-O bonds without opening or saturation of the aromatic ring^[77,78]. Transition metal Fe is a suitable catalyst for guaiacol hydrodeoxygenation.

Guaiacol is also considered a prospective feedstock for the production of cyclohexanol, which mainly involves the step of the splitting of C-O bonds and the hydrogenation of aromatic hydrocarbons. In 2021, Fe-based catalysts are prone to carbon deposition or carburization^[79]. To solve this problem, Li *et al.* introduce a trace amount of noble metal (including Pt, Ir, Pd, Rh, and Ru) into ceria-supported Fe catalysts. Among these single alloy catalysts, Pt-Fe/CeO₂ shows the highest catalytic activity. A very low amount (Pt/Fe = 0.01) provides sufficient activity. In particular, the addition of H₂O can improve catalyst stability without affecting the initial NM-Fe/CeO₂ activity and product distributions^[80]. After H₂O dissociates at the interface between metallic Fe atoms, the resulting hydroxyl group may further decompose into active O* species. The resulting O* can react with CH_x fragments, which serve as coke precursors formed from the overreaction of phenolic intermediates [Figure 9A]. In 2021, Xiang *et al.* reported a support-free RuCo catalyst capable of producing cyclohexane or cyclohexanone from guaiacyl molecules. The unique 3D pompon-like superstructure, achieved via a one-pot solvothermal integration path, facilitates baring active

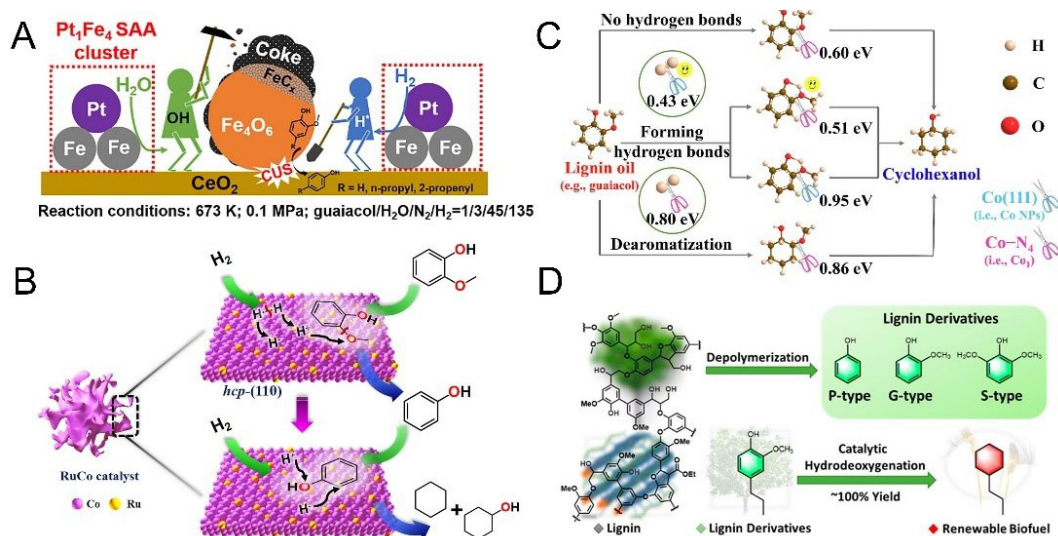


Figure 9. (A) Deactivation Mechanisms for Pt-Fe/CeO₂ Catalyst in the Absence of H₂O and in the Presence of H₂O^[80]. Copyright 2021 American Chemical Society; (B) Proposed possible mechanism for the guaiacol HDO over the hcp RuCo catalyst^[81]. Copyright 2021 Elsevier; (C) Hydrogenative C-O cleavage of lignin oil by a dual-size Co catalyst^[82]. Copyright 2023 Elsevier; (D) Reaction Route of the Catalytic Conversion from Lignin to Renewable Biofuel^[84]. Copyright 2024 American Chemical Society. HDO: Hydrodeoxygenation.

sites to provide more open pathways for diffusion of reactants and products [Figure 9B]^[81]. Similar to previous work, Zhang *et al.* used a metal-organic framework (MOF) as a precursor to obtain dual active site materials nCo_{1-n}NPs@NC with Co₁ and Co_{NPs} loaded. Whereas the original reaction (route a) allowed the removal of aromatics, the present catalyst is capable of efficiently and selectively cleaving the CAR-OCH₃ bond (route b) [Figure 9C]^[82]. Recently, Guo *et al.* reported a Ni-based catalyst Ni₁/β-Mo₂C which achieved 100% conversion for the hydrodeoxygenation of dihydroeugenol (DHE) to sustainable biofuels^[83]. The same catalyst was used for the hydrodeoxygenation of guaiacol, producing similarly excellent results. DFT calculations show that the introduction of Ni single atoms changes the adsorption site and adsorption pathways of the aromatic ring. The same catalyst was used for the hydrodeoxygenation of guaiacol, producing similarly excellent results. DFT calculations show that the introduction of Ni single atoms changes the adsorption site and adsorption pathways of the aromatic ring. As illustrated in Figure 9D, the first active site, the Ni single atom, absorbs DHE.

In another study, Zhang *et al.* reported that Ru, an atom supported on cerium dioxide (CeO₂) with a lamellar morphology, catalyzes the hydrogenation of the benzene ring structure to obtain cyclohexanol [Figure 10A]. X-ray diffraction (XRD) patterns show that the synthesized CeO₂ samples and catalysts exhibit well-defined diffraction peaks of standard CeO₂ samples and expose 110, 100 and 111 facets, which may be beneficial for catalysis [Figure 10B1-B2]. The aberration-corrected high-angle annular dark-field scanning TEM (HAADF-STEM) images and corresponding energy dispersive X-ray spectrometry (EDS) mapping show that Ru or other metal species disperse homogeneously and exist as isolated single atoms on the CeO₂ supports [Figure 10B3-B4]. The FT of EXAFS demonstrates the coordination result of Ru-O-Ce [Figure 10C1-C3]. XPS spectra indicate that the atomic Ru leads to more oxygen vacancies on the Ru/CeO₂-S surface, where the oxygen vacancies can positively contribute to the hydrodeoxygenation reaction of aromatic hydrocarbons by promoting hydrogen activation, adsorption and transfer of reactive hydrogen atoms [Figure 10C3-C5]. The interfacial cooperation between a single Ru atom and CeO₂. The Ru-O-Ce active site is formed by the coordination of one Ru atom with four O atoms, which can effectively activate the structural hydrogen of the benzene ring and thus promote the selective hydrodeoxygenation of

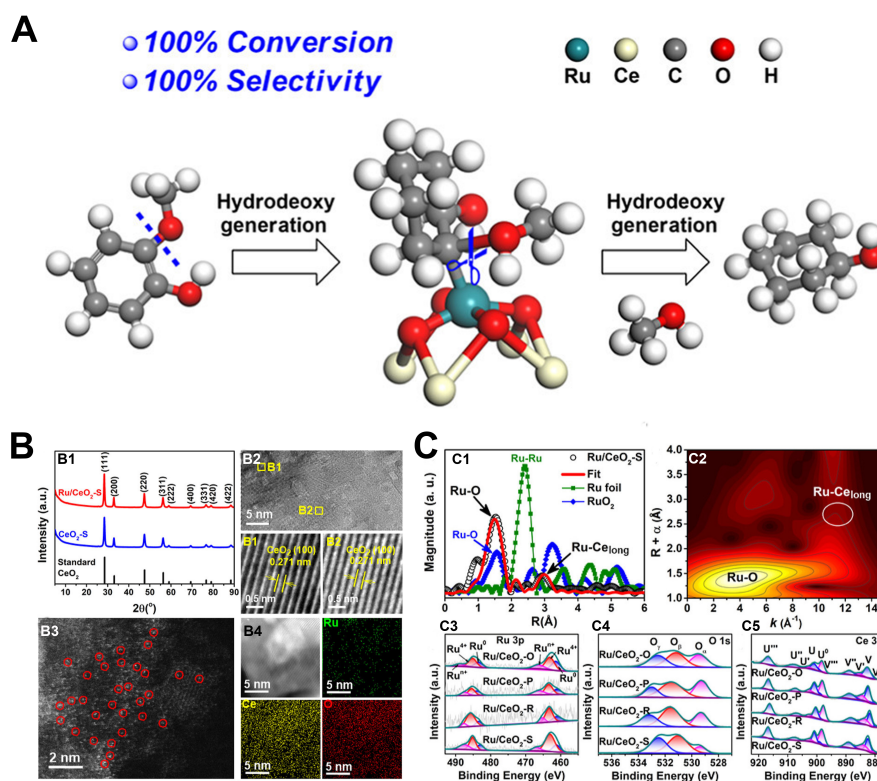


Figure 10. (A) Ru/CeO₂-S Schematic of catalysis; (B) B1: XRD patterns of the CeO₂-S sample (blue) and Ru/CeO₂-S catalyst; B2: TEM image of the Ru/CeO₂-S (red); B3: HAADF-STEM image of the Ru/CeO₂-S; B4: HAADF-STEM image and the corresponding EDS mapping of the Ru/CeO₂-S; (C) C1: FT k₃-weighted Ru K-edge EXAFS spectra; C2: Wavelet transform of the Ru K-edge EXAFS spectrum; C3-C5: XPS spectra of the Ru/CeO₂ catalysts for Ru 3p, O 1s, and Ce 3d regions^[82]. Copyright 2022 American Chemical Society. HAADF-STEM: High-angle annular dark-field scanning TEM; EDS: energy dispersive X-ray spectrometry; XRD: X-ray diffraction; EXAFS: extended X-ray absorption fine structure; XPS: X-ray photoelectron spectroscopy.

aromatic hydrocarbons in the reaction^[84].

Native lignin

Depolymerization of real lignin without a chemical pretreatment is challenging. Many efforts have been made to enable the direct application of these biomass feedstocks containing large amounts of phenolic monomers. Chen *et al.* reported an efficiency SAC comprising single Pt atoms on Ni NPs supported on carbon (Pt₁Ni/C). Using this catalyst, a lignin monomer yield of 37% from birch sawdust was achieved under 5 MPa H₂ in MeOH at 200 °C. Compared to other published mental catalysts, such as single Pt atoms catalysts (Pt₁/C) or Ni NPs catalysts (Ni/C), Pt₁Ni/C has significant catalytic activity [Figure 11A]^[85]. In another study, based on the cleavage of β-aryl ether bonds, Meng *et al.* reported a synergistic catalyst that integrates atomically dispersed Mo centers and Al Lewis acid sites on a MgO substrate (Mo₁Al/MgO). The catalyst's efficiency was tested using the model compound guaiacyl glycerol-β-guaiacyl (GG) as a template. The results showed that Mo loading higher than 3.0 wt% led to the aggregation of Mo species and reduced catalytic activity. Additionally, the reaction over Mo₁Al/MgO was found to be greatly influenced by the protic solvent. Subsequently, the improved catalyst system can be used for the direct depolymerization of lignin in eucalyptus. As we can see in Figure 11B, the optimum yield of monophenolics reached 46% with 92% selectivity, which was very close to the theoretical yield. DFT calculations and catalytic tests have shown that the Mo1-O5 center and the exposed Al Lewis acid site acted synergistically. Following guaiacol

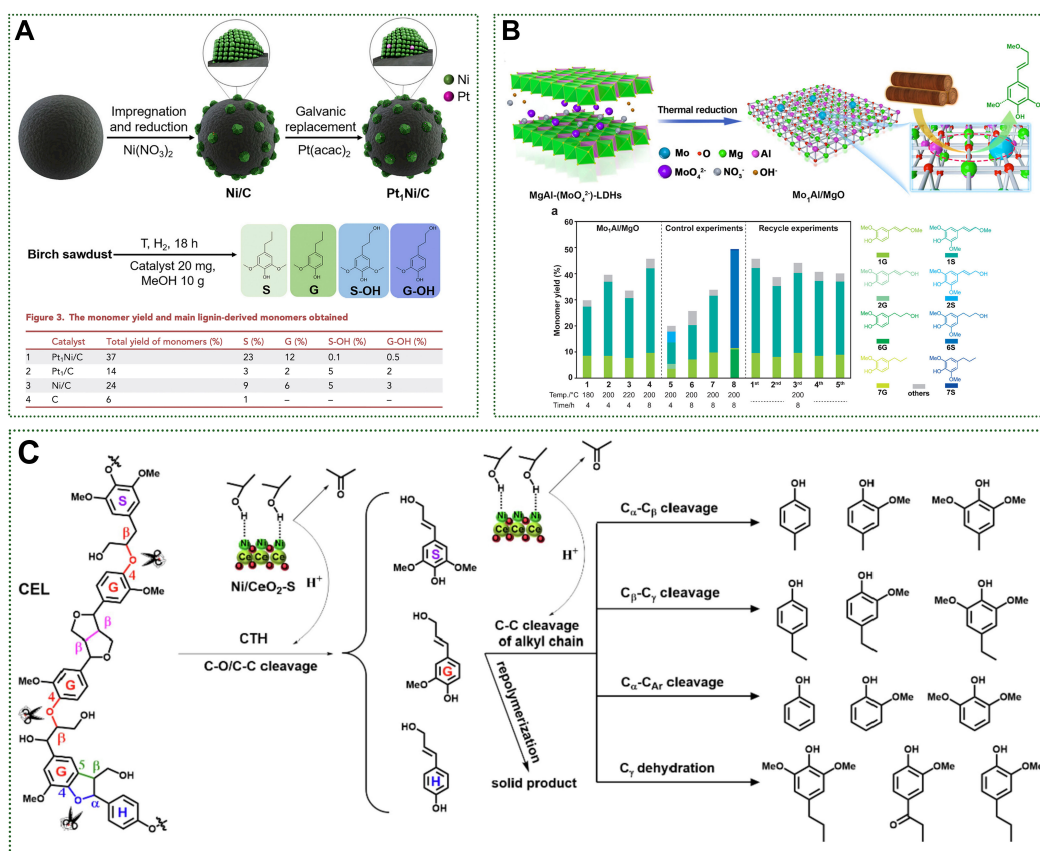


Figure 11. (A) Route used to prepare the Pt,Ni/C catalyst (up) and the monomer yield and main lignin-derived monomers obtained. Reaction conditions: 0.1 g birch sawdust, 0.02 g catalyst, 5 mL MeOH, 5 MPa H₂, 200 °C, and 18 h (down) [85]. Copyright 2019 Elsevier; (B) Schematic illustration of the confinement strategy to synthesize the Mo_{0.4}Al/MgO catalyst for selective lignin disassembly over synergistic Mo single-atom and Al Lewis acid sites (up). And Lignin depolymerization performances at different reaction conditions in methanol under N₂ (down) [86]. Copyright 2023 American Chemical Society; (C) Schematic diagram of CEL catalytic transfer hydrogenolysis over 1.0Ni/CeO₂-S catalyst [90]. Copyright 2022 Elsevier. CEL: Cellulolytic enzyme lignin.

formation and desorption, the O* intermediate formed stabilizes and acts as an oxidizing agent converting coniferyl alcohol to coniferyl aldehyde and coniferyl methyl ether [86].

Catechyl lignin (C-lignin) is a homopolymer biosynthesized from caffeyl alcohol owing to the lack of O-methyltransferase [87,88]. Due to its stable structure property, C-lignin can be extracted directly from plant material without condensation; at the same time, a large number of catechol skeletons appear in various pharmaceuticals and functional materials. Thus, C-lignin is well-suited feedstock for biomass conversion. Wang *et al.* reported a catalyst anchoring Ru clusters or single atoms in MOFs, demonstrating significant activity in the hydrogenolysis of C-lignin, resulting in the production of catechol monomers with high yields and high turnover numbers. Using C-lignin isolated from castor seed endocarp as a sample, Ru/ZnO/C demonstrated superior catalytic performance in parallel experiments, significantly outperforming commercial Ru/C in catechol production. The highest yield of monomeric catechols reached 81% under modified reaction conditions [89]. In another study, Jiang *et al.* described an effective approach for transforming cellulolytic enzyme lignin (CEL) through depolymerization and hydrodeoxygenation. Hydrogen activated at the Ni site targets the C-O and C-C bonds in CEL, producing intermediates such as sinapyl, coniferyl, and p-coumaryl alcohols. These intermediates are predominantly converted into stable methoxyphenol through the cleavage of the C-C bonds in the alkyl chain, facilitated by a Ni/CeO₂-S catalyst

[Figure 11C]. A maximum LO and monomer yield of 84.3 wt% and 32.6 wt%, respectively, was achieved at 260 °C for four hours. The LO obtained a higher heat value of 31.64 MJ/kg compared to CEL^[90].

others

Glycerol, a derivative of the biofuel industry, is currently facing an overproduction issue. The directed oxidation of alcohols to aldehydes and acids represents an essential procedure within the chemical transformation, offering a sustainable route for producing high-value chemicals and fuels from biomass resources^[91-95]. Glycerol, a highly functionalized molecule characterized by the presence of both primary and secondary hydroxyl groups, can serve as a precursor to many high-value products. In thermal catalysis, monoatomic catalysts are more effective in the hydrogenolysis of glycerol to 1,3-propanediol. Cinnamaldehyde and crotonaldehyde are two of the most important biomass-derived aldehydes that can also efficiently complete the corresponding reactions, such as oxidation or hydrogenation, under the catalysis of SACs to produce more valuable downstream products. Finally, we mentioned the reductive catalytic fractionation (RCF) strategy. The low binding energy of natural lignin and the high number of condensation bonds of industrial lignin are both unfavorable for lignin depolymerization, but RCF allows the heterogeneous catalytic conversion of natural lignin from wood under relatively mild conditions, resulting in almost theoretical yields of lignin-derived phenolic monomers (LDPMs) and recovery of pulp-rich solids and high-purity whole cellulose^[96-98]. Currently, this approach remains challenging.

Glycerol

Glycerol has become a cheaper and more available biomass platform chemical since the expansion of biodiesel production^[91-93]. Converting glycerol from biodiesel into high-value chemicals is a suitable strategy for dealing with the surplus supply. The compound 1,2-propanediol produced by breaking the C-C and/or C-O bond is a significant product of the hydrogenolysis of glycerol and also a significant industrial material^[94,95]. In 2016, Wang *et al.* started research about Pt-based SAC catalyst supported on mesoporous WO_x. However, this material cannot be considered a standard SAC, the excellent carrier for platinum structures rich in oxygen vacancies and hydroxyl functional groups due to the dispersion of platinum species on an atomic or pseudo-atomic scale^[99]. The least unoccupied molecular orbitals (LUMOs) of tungsten (W) can accept an electron from hydrogen (H), resulting in the formation of Hδ⁺ and leading to the development of Brønsted acidity. Meanwhile, the Pt site triggers concerted dehydration-hydrogenation reaction. As a result, it is favorable to the bond formation between glycerol and WO_x; meanwhile, more steady secondary carbocation intermediate formation makes it possible to produce 1,3-propanediol instead of 1,2-propanediol. Later, Zhang *et al.* continued the research about bimetallic alloy catalysts for the hydrogenolysis of polyols; a PtCu-SAA catalyst was successfully prepared. As shown in Figure 12A, both Pt/MMO and Cu/MMO catalysts showed low conversion rates (14.5% and 38.9%), while the PtCu-SAA sample displayed significantly enhanced catalytic performance (almost complete conversion and selectivity) at 200 °C and 2 MPa H₂ pressure. The ln (CA⁰/CA) versus reaction time plots are a straight line starting from the origin [Figure 12B], signifying a pseudo-first-order reaction associated with glycerol. The main secondary products are ethylene glycol and n-propanol, resulting from C-C bond cleavage and excessive hydrogenolysis, respectively [Figure 12C]. Finally, the TOF of the PtCu-SAA catalyst was ~ 150 and 14 times higher than that of the single Cu and Pt-based catalysts [Figure 12D]^[100]. The preparation of the catalytic material and the catalyzed reactions are shown in Figure 12E.

The selective oxidation of glycerol to glyceric acid constitutes a significant value-added reaction for polyols. An *et al.* designed a sequential co-catalysis method for the selective oxidation of glycerol to glyceric acid in which a single platinum atom synergizes with a low-coordinated Pt-Pt. In this work, the whole reaction is

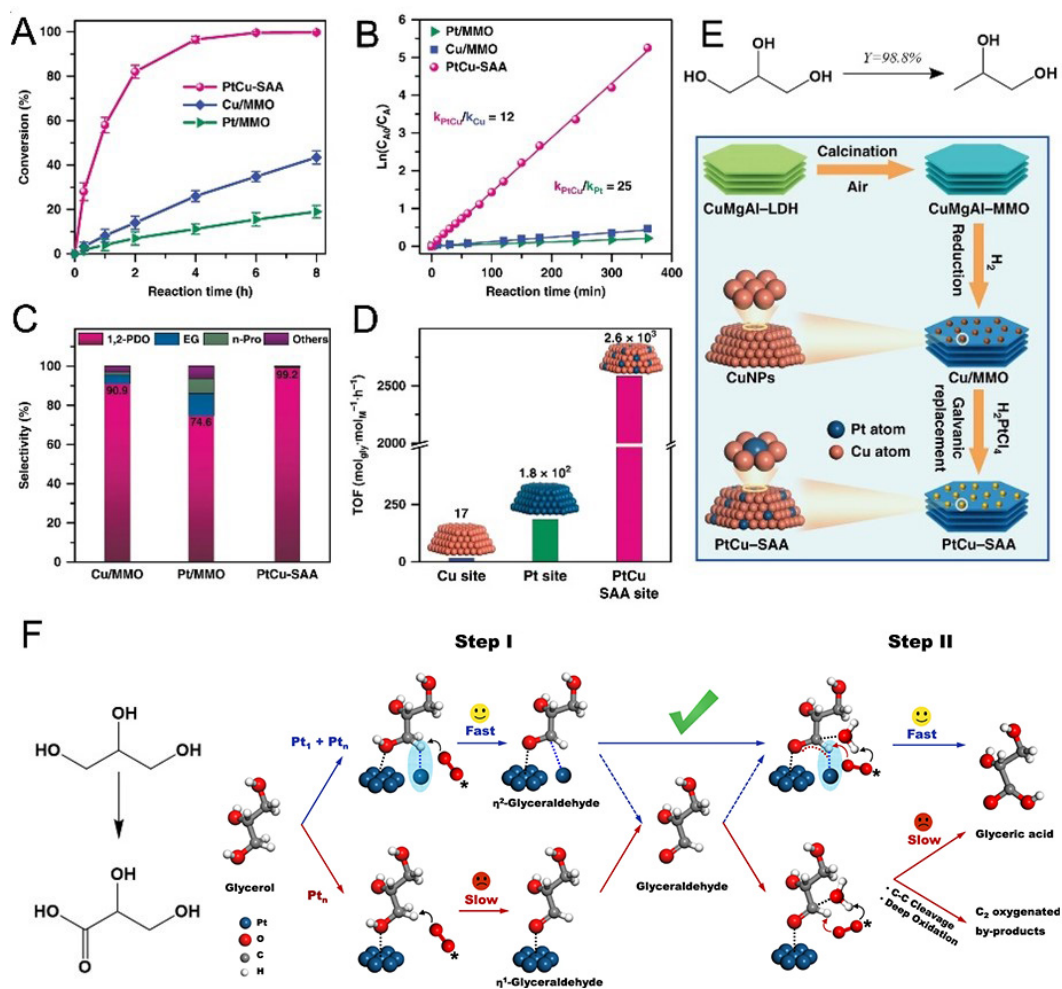


Figure 12. (A-E) Catalytic evaluation of PtCu-SAA and monometallic catalysts (Pt/MMO and Cu/MMO) toward glycerol hydrogenolysis to 1,2-PDO^[100]. Copyright 2019 Springer Nature. (F) Atomic Pt₁ site provides an enhanced C-H activation (marked in blue shade) in the cascade synergy, forming the η^2 -adsorbed GLAD^[101]. Copyright 2022 Springer Nature. SAA: Single-atom alloy; GLAD: glyceric acid; PDO: 1,2-Propanediol.

divided into two processes: the oxidation of glycerol to glycerol aldehyde and the oxidation of glycerol aldehyde in series to glycerol acid as described in Figure 12F. It enhances C-H activation on atomic Pt₁ and O-H activation on cluster Pt_n, facilitating the oxidation of in the tandem cooperative catalytic system. It also enables cluster Pt_n to activate C=O, and, subsequently, O-H insertion^[101]. The results indicated that it demonstrated a high level of catalytic activity with glycerol conversion (90.0%) and glyceric acid selectivity (80.2%).

Crotonaldehyde

Selective hydrogenation of α,β -unsaturated aldehydes into unsaturated alcohols is a promising application for heterogeneous catalysts. However, precise adsorption and effective activation of C-O bonds remain significant challenges. Inspired by the unique spatial effect of the pocket-like structure of the enzyme reactive center, Lou *et al.* designed a pocket-like active site by anchoring single Rh atoms to the Mo edge vacancies of 2D MoS₂ sheets [Figure 13A]^[102]. DFT calculations show that the oxygen atoms of the 2D MoS₂

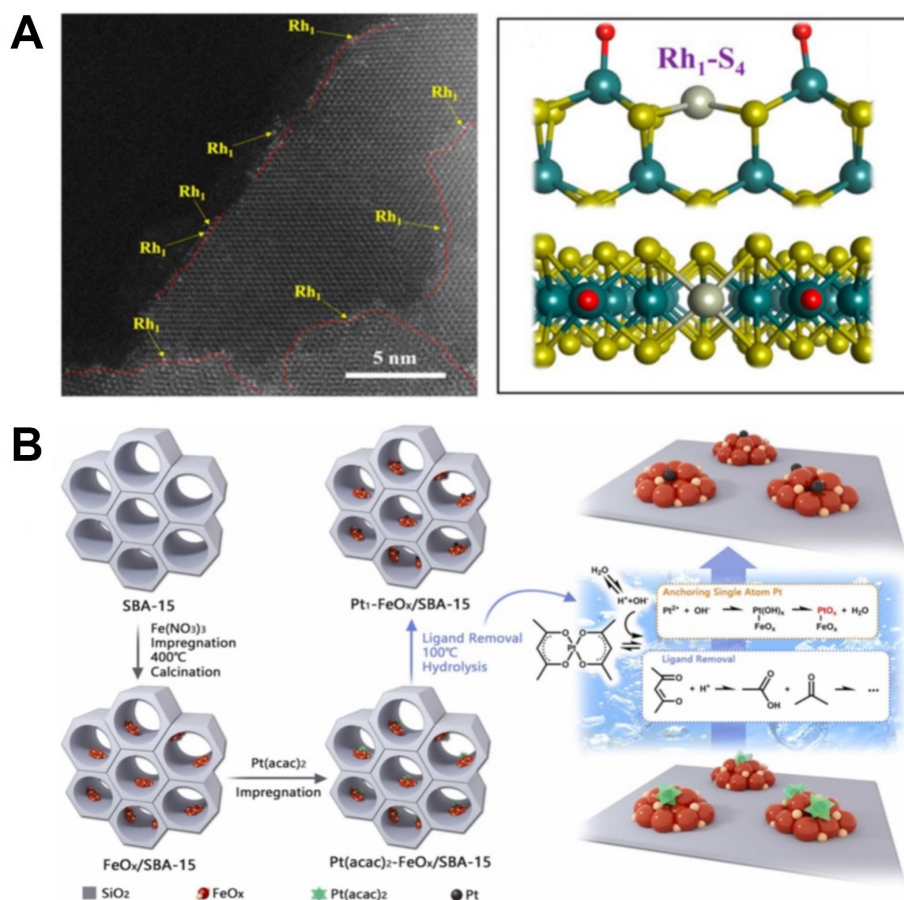


Figure 13. (A) Representative atomic resolution HAADF-STEM images of the as-synthesized Rh_1/MoS_2 SAC. (left) Schematic of the structure of Rh_1/MoS_2 SAC. The white dots (indicated by the yellow arrows) in the HAADF-STEM images represent single Rh_1 atoms. (right) Copyright 2019 American Chemical Society; (B) Illustration of synthetic procedure of $\text{Pt}_1\text{-FeO}_x/\text{SBA-15}$ catalyst under mild conditions^[108]. Copyright 2023 Elsevier. HAADF-STEM: High-angle annular dark-field scanning TEM; SACs: single atom catalysts.

are bonded to Mo atoms, and the pocket-shaped structure leaves the Rh_1 active site exposed to better bind and dissociate from the hydrogen molecules, which are then released along the edges to form OH groups. This results in a unique configuration: $\text{HO-Mo-Rh}_1\text{-Mo-OH}$. This unique active site not only catalyzes the hydrogenation of hoods to crotonols, but also has 100% selectivity. Afterwards, this group did similar work by turning the metal in the active site into Pt, also achieving excellent catalytic effect^[103].

Cinnamaldehyde

The metals, Pt, Ni, Ru, Cu, etc., are commonly used as catalysts for the hydrogenation of cinnamaldehyde^[104-109]. Li *et al.* presented a series of work about Pt-based SACs for cinnamaldehyde conversion. For example, Pt atoms anchored on CeO_2 nanorods with abundant oxygen vacancies demonstrated outstanding catalytic performance: 99% conversion and a TOF of $2,410 \text{ h}^{-1}$ for styrene hydrogenation, 99% conversion and selectivity with a TOF of 968 h^{-1} for cinnamaldehyde hydrogenation, and 99% conversion with 79% selectivity and a TOF of $10,000 \text{ h}^{-1}$ for triethoxysilane oxidation. Notably, this synthetic method can be scaled up without compromising catalytic performance, making it suitable for industrial applications^[104]. After that, hexagonal boron nitride nanosheet and defect-containing $\beta\text{-FeOOH}$ can also anchor Pt atoms to construct Pt SACs, where rational use of nitrogen-containing vacancies and

oxygen vacancies stabilizes Pt atoms^[106,107]. In a recent study, the manufacturing of single-atom Pt catalysts was first reported using SBA-15 covered with functional FeO_x nanoclusters as support through a mild hydrolysis technique. They first proposed using Pt acetylacetonate as a precursor, which is treated hydrothermally to remove the ligand, leaving the single metal atom [Figure 13B]. Attributed to the synergistic effect between isolated Pt atoms with high surface positive charges and FeO_x nanoclusters on SBA-15, the further hydrogenation of cinnamaldehyde was inhibited^[108].

Reductive Catalytic Fractionation of Lignocellulosic

Lignocellulosic biomass offers a promising substitute for fossil resources, attributed to its structural complexity and the abundant availability of raw materials. RCF is an efficient and separable method for converting lignin biopolymers into monomeric phenols. Guided by the lignin-first strategy, the combining of RCF and non-homogeneous catalysts to improve harsh reaction conditions is a highly potential field of research for upgrading biomass.

In 2020, Park *et al.* reported an extremely low Pd-loaded (0.25 wt%) CN_x supported catalyst capable of achieving LDPM carbon yield and completely delignified holocellulose recovery of 52.7 C% and 84.2 wt%. As shown in Figure 14A, the size of the loaded metal affects the reaction process. Compared to Pd5/AC catalyst, Pd_{0.25}/CN_x shows better industrial applicability and higher activity in hydrodeoxygenation and double-bond saturation, producing 4-n-propyl guaiacol/syringol as major products. Various types of biomasses were tested to demonstrate the effectiveness of Pd_{0.25}/CN_x for biomass fractionation^[110]. 2022, a type of Co-based SAC was also synthesized using a mixture of lignin-metal complex and melamine as the precursor, which was adopted for acid-assisted reductive fractionation of lignocellulose in the presence of 0.1% sulfuric acid without H₂. Due to the synergistic effect of metals and acids, a satisfactory monophenol yield of 41.7% was obtained along with nearly complete delignification at 99.7%^[111]. In another research, Song and his group reported a highly dispersed Ru anchored on a chitosan-derived N-doped carbon catalyst (RuN/ZnO/C) with high selectivity towards propyl end-chained guaiacol and syringolis, also 20 times higher than the commercial Ru/C catalysts. Using birch wood chips, RCF at 240 °C with H₂ in MeOH (3 MPa at 25 °C) produced a number of monomers, dimers and oligomers, as well as an insoluble fraction consisting of cellulose (C6 sugars), hemicellulose (C5 sugars) and catalysts^[112]. Selectively oxidative the cleavage of the C(O-)-C bond present in lignocellulose offers a more cost-effective and straightforward way of converting biomass feedstocks into relatively high yield carboxylic Acids. This study introduced Ir atoms into carboxylic acid on NiFeO, the electrochemical transformation of carbohydrates and lignin model compounds [Figure 14B]. The Ir-NiFeO@NF catalyst exhibited exceptional dual functionality, surpassing performance in both lignocellulose oxidation [≤ 1.35 V vs. reversible hydrogen electrode (V_{RHE})] and hydrogen evolution (26 mV). This led to an overall cell efficiency requiring merely 1.33 V_{RHE} at 10 mA cm⁻²^[113].

Electrocatalysis

As previously discussed, the main approach for biomass conversion is thermochemical catalysis, which necessitates elevated temperatures and pressures. With the rising cost of renewable energy and the demand for milder reaction conditions, electrochemical processes are becoming a viable pathway^[114]. Electrocatalysis uses electrons as redox agents without the need for additional oxygen or hydrogen sources, providing a clean and efficient conversion strategy. SACs can also be employed in the electrocatalytic conversion of biomass. More generally, the advantages of electrocatalysis can be considered from the following aspects. First, the electrocatalysis can be carried out with a simple device at room temperature and atmospheric pressure; the selectivity and conversion can be controlled by adjusting the applied potential, electrode

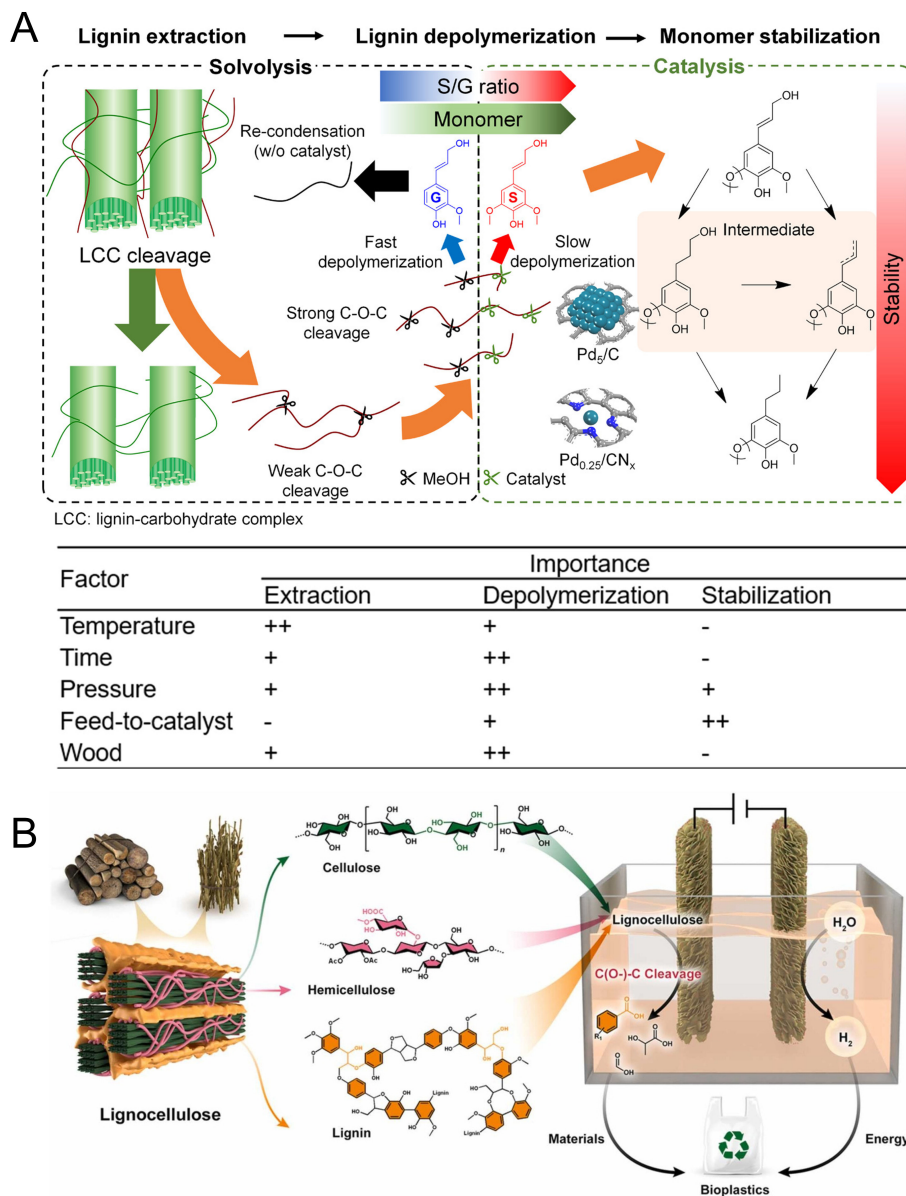


Figure 14. (A) Schematic of the RCF of wood over the $\text{Pd}_{0.25}/\text{CN}_x$ catalyst with importance of reaction factors toward lignin extraction, depolymerization, and stabilization^[110]. Copyright 2020 American Chemical Society; (B) The overall sustainability concept of lignocellulose upgrading reformation and application^[113]. Copyright 2023 Elsevier. RCF: Reductive catalytic fractionation.

material and electrolyte^[115]. Secondly, coupling biomass valorization with CO_2 conversion through electrocatalysis offers a promising method to simultaneously produce valuable commodity chemicals at both electrodes^[116-118]. Furthermore, electrochemical catalysis can be driven by clean energy generation such as solar power, which offers a hopeful approach for the development of green technology. Statistically, both noble metals such as Ir, Ru, Rh, Co and non-precious Cu metals loaded on different carriers can provide suitable active sites for electrocatalysis. Until now, most of the reactions are transformations of HMF, such as oxidation, hydrogenation, and hydrogenolysis reactions; a few SACs are used for electrochemical reduction and coupling reactions of furfural or glycerol.

HMF oxidation

DHMF, catalytically reduced by HMF, acts as a crucial starting material for the creation of various functionalized polymers such as polyethers, polyurethanes, and polyamides^[119]. Pure metal electrodes (Cu, Bi, Pb) remain inactive at high voltages, which hinders the reactivity. In 2022, Ji *et al.* introduced a Ru₁Cu SAA catalyst for HMF conversion to DHMF. Firstly, the copper foam was chemically oxidized to obtain CuO nanowires arrays, and then Ru₁Cu SAA with different Ru loadings were obtained by varying the concentration of RuCl₃ and the duration of substitution. This catalyst exhibited increased activity and faradaic efficiency (FE) at a lower potential; the FE (87.5%) is largely maintained even at high HMF concentrations (100mM). Therefore, the atomic Ru plays a crucial role in facilitating the water dissociation, thereby increasing the surface concentration of H⁺, and the Cu counterparts are fascinating in the electronic transfer process. This, in turn, reduces the carbonyl group of HMF, leading to the production of DHMF via an electrochemical hydrogenation (ECH) mechanism^[120].

The oxidation products of HMF, FDCA and DFF serve as precursors for the polymer industry and as valuable byproducts in the transformation of fatty acids into biodiesel. In 2021, Lu *et al.* were able to enhance the overall conversion rate of HMF by modulating the adsorption of HMF as demonstrated in [Figure 15]. They tried to maximize the HMF adsorption behavior on spinel oxides (Co₃O₄) by introducing single atom Ir. The linear sweep voltammetry curves reveal exceptional HMFOR performance for Ir-Co₃O₄, with a lower onset potential (1.15 V_{RHE} at 1 mA cm⁻²) and higher current density compared to Co₃O₄ (1.35 V_{RHE}) and other reported HMFOR catalysts. Temperature programmed desorption (TPD) measurements were conducted to study HMF adsorption behavior. Results indicated that Ir-Co₃O₄ exhibited a higher desorption temperature for HMF molecules than Co₃O₄, suggesting stronger HMF adsorption. TPD experiments in ethylene and carbon monoxide atmospheres further demonstrated stronger adsorption of C=C groups on Ir-Co₃O₄. Consequently, the lower binding energy reduces the kinetic barrier, accelerating the HMFOR process. Two potential pathways for HMFOR were considered; potentiostatic electrolysis at 1.42 V_{RHE} and quantification of HMF, HMFCA, DFF, 5-formylfuroic acid (FFCA), and FDCA revealed pathway I predominates. Additionally, Ir-Co₃O₄ showed a higher yield and FE (98%) compared to Co₃O₄. This study demonstrates that single-atom Ir on Co₃O₄ enhances the electro-oxidation of organics by improving adsorption capacity, offering a novel strategy for designing efficient electrocatalysts^[121].

In another work, single-atom ruthenium nickel oxide (Ru₁-NiO) was used as a catalyst for the efficient electro-oxidation of HMF in a neutral medium, which breaks through the traditional limitations of alkaline media^[122]. Figure 16A illustrates the catalytic mechanism of the catalyst. The adsorption of water molecules on Ru atoms results in the dissociation of OH⁻ species, accompanied by electron and proton transfer. Subsequently, OH⁻ reacts with a nucleophilic reagent (Nu), namely HMF, to produce DFF and water. A deeper insight into the HMFOR mechanism was gained using cyclic voltammetry (CV) analysis. From the CV curve of NiO in 1.0 M phosphate-buffered saline (PBS), it can be seen that an oxidation peak appears in the region of 0.8 V < E < 1.1 V, which is consistent with the OH⁻ adsorption region reported in the literature. More critically, the onset potential of hydrolysis dissociation is consistent with that of HMFOR, suggesting that the OH⁻ substance produced by hydrolysis dissociation, rather than OH-oxidation, is the main active substance of HMFOR on NiO. This phenomenon was also observed for Ru₁-NiO, suggesting a similar reaction mechanism. The structural evolution of the catalyst at different potentials was traced using non-in situ Raman spectroscopy. No signal for Ni(III) was observed from Raman spectra after electrocatalysis in 1.0 M PBS at 1.3, 1.5 and 1.7 V, suggesting negligible surface oxidation of NiO at neutral pH. Raman spectra recorded in the presence of HMF showed similar results [Figure 16B-E].

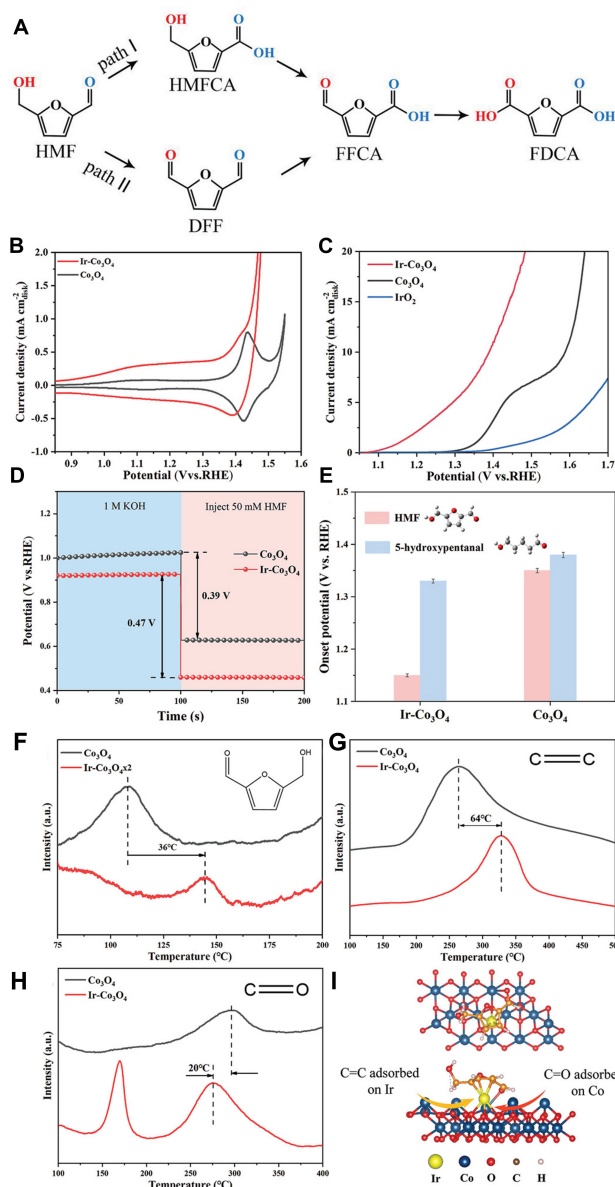


Figure 15. (A) Two possible reaction pathways for HMF oxidation; (B-E) The electrochemical activity of Ir-Co₃O₄ and Co₃O₄; (B) CV curves of Ir-Co₃O₄ and Co₃O₄ in 1 M KOH at a scan rate of 5 mV s⁻¹; (C) LSV curves of Ir-Co₃O₄, Co₃O₄, and IrO₂ in 1 M KOH with 50 × 10⁻³ M HMF at a scan rate of 5 mV s⁻¹; (D) OCP curves of Ir-Co₃O₄ and Co₃O₄ were subsequently measured in 1 M KOH and 50 × 10⁻³ M HMF; (E) Onset potential of Ir-Co₃O₄ and Co₃O₄ for HMFOR and hydroxypentanal electro-oxidation, respectively; (F-I) Adsorption evaluation for Ir-Co₃O₄ and Co₃O₄; (F-H) TPD spectra of Ir-Co₃O₄ and Co₃O₄ at HMF/He (F), ethylene (G), and CO (H) atmospheres; (I) The adsorption model of HMF molecules on Ir-Co₃O₄^[121]. Copyright 2021 Wiley-VCH. HMF: 5-hydroxymethylfurfural; CV: cyclic voltammetry; HMFOR: 5-hydroxymethyl furfural oxidation reaction; TPD: temperature programmed desorption; OCP: open circuit potential; KOH: potassium hydroxide.

Recently, Zhou *et al.* designed a single atom electrocatalysts (SAECs) composed of single Co atoms supported on nitrogen-doped carbon nanosheets (Cu/NCNSs)^[123]. Based on *in-situ* Raman spectra and high-performance liquid chromatography (HPLC) results, it can be shown that HMF oxidation on Cu NPs follows the path to DFF at lower potentials, shifting to the 5-hydroxymethyl-2-furan carboxylic acid (HFCA) pathway when the applied potential exceeds 1.67 V. Simultaneously, Zeng *et al.* described a series of Rh-O₅/Ni(Fe) atomic sites on nanoporous mesh-type layered double hydroxides, with atomic-scale

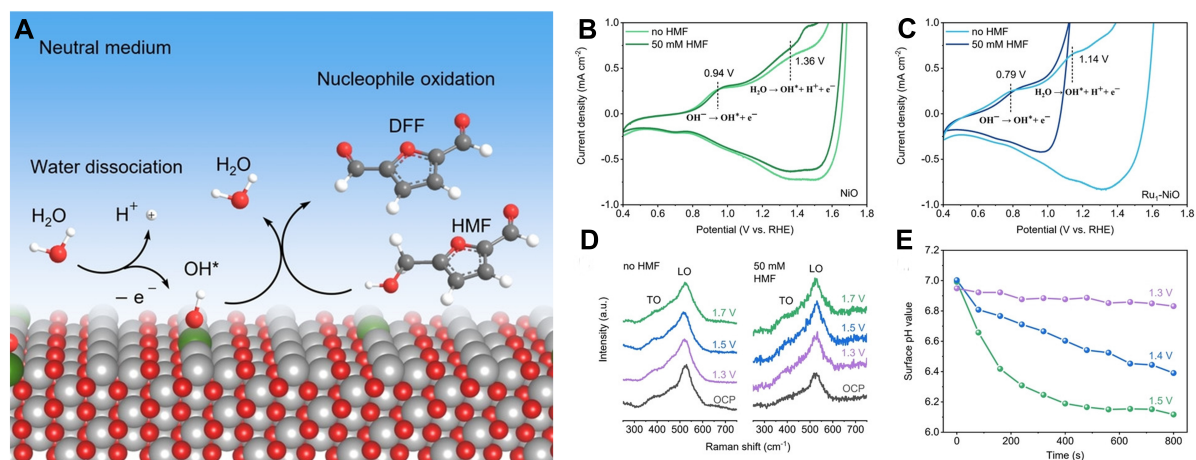


Figure 16. (A) Proposed HMFOR mechanism over $\text{Ru}_1\text{-NiO}$ in the neutral medium; (B-D) Investigations of HMFOR mechanism over $\text{Ru}_1\text{-NiO}$. CV curves of (B) NiO and (C) $\text{Ru}_1\text{-NiO}$ in 1.0 M PBS with and without 50 mM HMF; (D) The ex-situ Raman spectra of $\text{Ru}_1\text{-NiO}$ after electrocatalysis of 5 minutes; (E) Calculated surface pH values for $\text{Ru}_1\text{-NiO}$ [122]. copyright 2022 Wiley. HMFOR: 5- hydroxymethyl furfural oxidation reaction; PBS: phosphate-buffered saline; HMF: 5-hydroxymethylfurfural; CV: cyclic voltammetry.

cooperative adsorption centers that demonstrate high activity and stability in catalyzing alkaline HMFOR and hydrogen evolution reaction (HER)^[118]. In an integrated electrolysis system, achieving a current density of 100 mA cm^{-2} requires a low cell voltage of 1.48 V, accompanied by excellent stability over 100 h. From a thermocatalytic perspective, HMFOR is considered a tandem reaction with multiple intermediate products, requiring various active sites to enhance overall response efficiency.

Others

Mukadam *et al.* reported a good strategy for the electrocatalytic reduction of furfural to generate hydrofuran. Cu/Co-doped phthalocyanines are the case of single atom molecular catalysts that exhibit high selectivity for the electroreduction of furfural to hydrofuroin^[124]. Compared to RHE, hydrofuran produced a faradic efficiency of up to 65.3% at pH 10 and 0.50 V with low hydrogen precipitation; furthermore, Co-based catalysts demonstrate better stability compared to other catalysts. The initial proton-coupled electron transfer (PCET) step that forms the FCHOH intermediate is vital for hydrofuroin production, rather than the subsequent coupling reaction over weak-binding single-atom molecular catalysts [Figure 17]. Therefore, the key to the preparation of catalysts for furfural reduction reaction is to increase the adsorption of furfural at the active site, which provides inspiration for biomass electrowinning.

A promising method to increase the value of biomass feedstocks by reducing oxygen content is electrochemical coupling of C-O bonds. In this study, the generalized adsorptive deposition method loaded monoatomic Au on top of spinel synergistic composites to prepare SAC($\text{Au-NiMn}_2\text{O}_4$). Atomically dispersed Au occupies the surface Ni^{2+} vacancies, reducing the benzaldehyde adsorption energy and thus benzaldehyde coupling to produce dibenzyl ether, with high dibenzyl ether selectivity and Faraday efficiency. Spinel nanostructures, as a new catalytic support material, will exhibit excellent catalytic performance in the field of single-atom electrocatalysis^[125].

Converting glycerol to higher value glycol aldehydes via glycerol oxidation is a promising study. Wang *et al.* utilized electrocatalysis to report a single atom bismuth (Bi) doping strategy. Experimental characterizations and theoretical calculations reveal that single-atom Bi substitutes cobalt at octahedral sites (CoOH^{3+}) in Co_3O_4 , facilitating the formation of reactive hydroxyl species (OH^*) at nearby tetrahedral Co sites (CoTd^{2+})

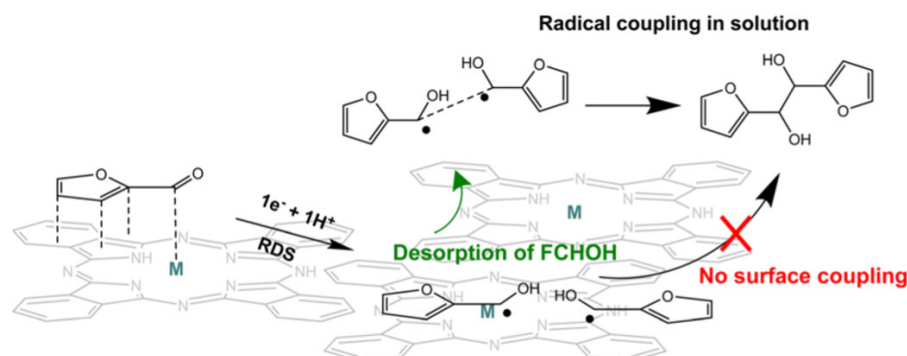


Figure 17. Proposed mechanism of hydrofuroin production in furfural reduction on metal-doped phthalocyanine where 'M' represents a metal atom/ion^[124]. Copyright 2023 Royal Society of Chemistry.

[Figure 18A]^[126]. Reactive OH* species can catalyze the cleavage of C-C bonds in glycerol via a direct oxidation mechanism, ultimately converting glycerol into glycolaldehyde [Figure 18B].

This example demonstrates the application of electrocatalytic oxidative cleavage of the C α -C β bond in lignin β -O-4 model compounds. Under optimized conditions (150 °C, 4 h) in MeOH solvent in air, a 95% conversion of MPP-ol was achieved. C-C bonds typically exhibit increased dissociation energy compared to C-O bonds in lignin. Therefore, targeted cleavage of the C-C bond without disrupting the benzene ring is a critical factor in lignin depolymerization. In this study, N-doped CNTs anchor a single-atom Pt catalyst which was used for selective C α -C β bond cleavage through electrocatalytic oxidation. Using 2-Phenoxy-1-phenylethanol as a model compound, Pt₁/N-CNTs exhibit exceptionally high C α -C β bond cleavage activity and selectivity, achieving an 81% yield of benzaldehyde. This performance surpasses the current state-of-the-art Pt electrode and Pt/C benchmark catalysts [Figure 19]^[127].

Photocatalysis

The catalytic conversion of lignocellulosic biomass using solar energy has recently garnered significant attention. This interest arises from the distinctive reactive species and reaction mechanisms initiated by photoexcited charge carriers or photogenerated reactive entities, along with the mild reaction conditions. These factors facilitate precise cleavage of lignocellulosic biomass^[10]. Photocatalysis typically begins with the absorption of light, which excites the photocatalyst to an elevated energy state. Conventional thermocatalysis relies on high-temperature activation to overcome energy barriers. Photocatalysis typically begins with the absorption of light, which excites the photocatalyst to a higher energy state. The excited photocatalyst can subsequently activate the reactant, surmounting the energy barrier and producing the desired products [Figure 20]. However, the conditions typically employed in thermocatalysis are often too rigorous to permit the selective activation of a specific functional group due to the multiple functional groups of the biomass reactants. Furthermore, thermal catalysis presents a challenge in conducting simultaneous reduction and oxidation reactions, such as the cleavage of the 1-bond in lignin, which necessitates a multistep conversion process. We propose that photocatalysis can address this challenge by enabling the selective transformation of specific reactants or the selective cleavage or functionalization of targeted chemical bonds or functional groups, while preserving other functional groups. Our findings indicate that the majority of SACs exhibit selective photocatalytic activity towards the C-O, C-H, and C-C bonds of biomass feedstocks by photocatalytic process. Specific studies are detailed in this chapter.

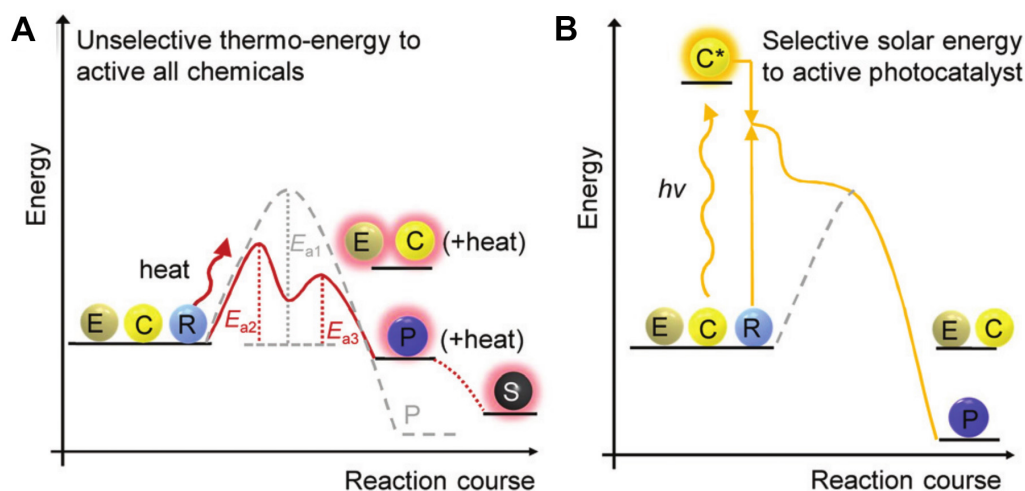


Figure 20. Energy diagram for the transformation of reactant (R) to product (P). (A) Thermocatalysis; (B) Photocatalysis, (C, E) and (S) refer to the catalyst, molecules in the environment, such as solvent and atmosphere, and byproducts, respectively^[10]. Copyright 2020 Royal Society of Chemistry.

production over 1 wt% Ru/Zn_{0.5}Cd_{0.5}S reached 17.4 $\mu\text{mol h}^{-1}$ and 17.1 $\mu\text{mol h}^{-1}$, respectively. The enhanced photocatalytic performance results from the highly efficient separation and transport of photoexcited charges, facilitated by the strong interaction between the Ru atom and Zn_{0.5}Cd_{0.5}S nanorods^[128].

In 2021, Lu *et al.* reported a photocatalytic method to simultaneously load Pt single atoms and nanoclusters onto silicoaluminophosphate-31 (SAPO-31) for the hydrodeoxygenation of vanillin. The high activity of the catalyst is due to the synergistic effect of strong metal-support interactions, facilitated by the simultaneous presence of isolated palladium atoms and clusters of palladium atoms^[129]. This catalyst exhibits unique geometrical and electronic properties, with synergistic effects due to the combination of single atoms and ultra-small nanoclusters, and also strong metal-carrier interactions contributing to better catalytic performance. Additionally, it shows almost 100% yield of production in the hydrodeoxygenation of vanillin to 2-methoxy-4-methylphenol (MMP) under barometric pressure with 80 °C and 30 min.

In another research, Ru single atom support on mesoporous carbon nitrides (Ru₁/MCN) was applied for selective oxidative cleavage of C α -C β bonds under visible light irradiation at room temperature; this method achieves almost complete conversion and high selectivity for C-C bond cleavage in 2-phenoxy-1-phenylethanol [Figure 21A]. A series of optical tests demonstrated the catalytic efficiency of Ru₁/MCN. Ru₁/MCN demonstrates significantly stronger light absorption in the visible region ($\lambda > 420$ nm) compared to MCN, as evidenced by ultraviolet-visible diffuse reflectance spectroscopy (UV-vis DRS) [Figure 21B]. As illustrated in Figure 21C, the intensity of the photoluminescence (PL) peak was markedly diminished following the incorporation of Ru on MCN. This observation implies that the addition of Ru single atoms facilitates the migration of photogenerated carriers while simultaneously suppressing the recombination of electron-hole pairs. Furthermore, the photocatalytic process unveils a mechanism involving carbon-centered radical intermediates. Firstly, photogenerated holes extract benzylic C β -H, resulting in the formation of a carbon radical intermediate. Simultaneously, O₂ is reduced to a free radical, coupling with C β radicals through a six-membered ring transition state. Following this, intra-ring electron transfer triggers the cleavage of the C α -C β bond, resulting in the formation of aromatic aldehydes and benzyl formate. Byproduct 2 arises from the oxidation of 1, which is more difficult to cleave because of the higher C α -C β bond energy in 2 [Figure 21D]^[130].

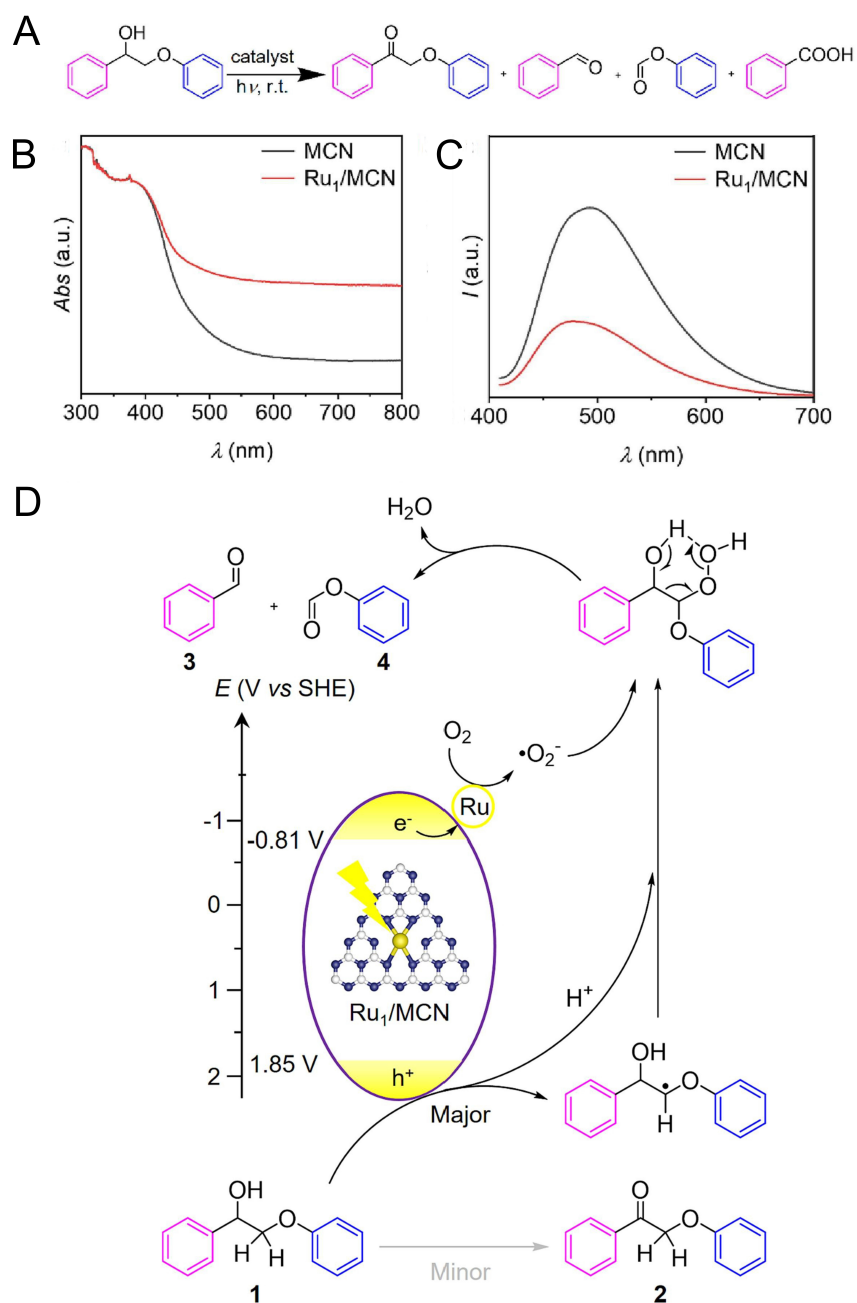


Figure 21. (A) Chemical molecular formula of the reaction; (B) UV-vis DRS spectra; (C) PL spectra; (D) Proposed mechanism of the photocatalytic depolymerization of 2-phenoxy-1-phenylethanol (1) through C_α-C_β bond cleavage using Ru₁/MCN SAC^[130]. Copyright 2023 Elsevier. UV-vis DRS: ultraviolet-visible diffuse reflectance spectroscopy; PL: photoluminescence; SACs: single atom catalysts.

In this scenario, the SACs consist of Ni single atoms anchored to the surface of titanium dioxide. Activated by light, the catalyst functions under ambient conditions, utilizing air as an eco-friendly oxidant. This process achieves a selectivity of over 60% for glycol aldehyde^[131]. The atomically dispersed nickel material anchored by the novel molten salt approach taken in this experiment exhibits significantly enhanced properties. Later, Xiong *et al.* employed visible light irradiation to convert glycerol into glyceraldehyde and dihydroxyacetone, achieving a high degree of selectivity. In this study, the non-precious metal copper was used in a highly reproducible manner by atomically dispersing it on the WO₃ surface. When glycerol

oxidation is carried out on this catalyst, photogenerated voids are activated and subsequently coupled to OH⁻, which eventually dehydrates to form the desired product^[132].

Ren *et al.* have turned their attention to biomass photoreforming hydrogen. The unstable hydrogen yield from biomass reforming is due to the intermittent nature of solar light and partial degradation of biomass C-C bonds. To address this issue, this study proposes the strategy of “C-C bond first” [Figure 22A], which utilizes carbohydrates from hydrolysis of lignocellulose as feedstock. First, biomass carbons are converted into liquid hydrogen carriers (LHCs) with nearly almost complete yield of C₁ products. Following degradation of the LHCs exclusively produces H₂ and CO₂. This strategy is realized using highly distorted Ta-doped CeO₂ (Ta-CeO₂), which effectively regulates C-C bond scission, C-C bond coupling, and the conversion of recalcitrant carbonyl compounds. The monosaccharides and biopolyols converted from cellulose and hemicellulose can be used for the preparation of C₁ LHCs by photocatalytic oxidation in yields ranging from 62% to 86%. The obtained aqueous solution of C₁ LHCs can be directly used for photocatalytic hydrogen production after simple filtration to remove Ta-CeO₂ catalysts. When Pt/P₂₅ is used as the photocatalyst or Ru-complex as the thermocatalyst for H₂ generation, LHCs are nearly completely decomposed, releasing H₂. The H₂ yields are 33% and 30%, respectively. In contrast, direct photocatalytic hydrogen production from glucose with Pt/P25 yielded only 13% H₂. Interestingly, the authors built a laboratory-scale flow reaction unit to demonstrate the feasibility of this scheme. After three days and a cumulative 15.5 h of sunlight, the C₁ LHCs yielded 15%, of which 19% of glucose was converted [Figure 22B-E]^[133].

Amino acids are traditionally prepared using biocatalytic methods, which have disadvantages such as time-consuming and difficult separation of products. Thus, Li *et al.* reported a sustainable method for the production of amino acids from biomass-derived hydroxyacids by loading atomic-level ruthenium onto cadmium sulphide (Ru₁/CdS), making the reaction highly active under visible light irradiation and mild conditions. Experimental and theoretical calculations show that atomically dispersed Ru sites on CdS nanosheets significantly improve carrier separation and transfer, inhibit hydrogen precipitation side reactions, and promote the dissociation of O-H bonds in the α -hydroxyl group of lactic acid. The rate of alanine production was 1.7 times greater and over two orders of magnitude higher compared to NPs and conventional thermal catalysis^[134].

Photoelectrocatalysis

Photoelectrochemical (PEC) biomass conversion is a sustainable, energy-efficient synthetic route driven by renewable energy under mild conditions^[135-137]. Photoelectrocatalysis uses solar energy to convert raw materials into target products; similar to photocatalysis and electrocatalysis, it possesses the advantages of low cost, green and energy saving. In recent years, photoelectrocatalysis has emerged as a promising approach in the field of biomass. The published studies have focused on the oxidation of various biomass alcohols/aldehydes, including glycerol and glucose. In addition, PEC technology can directly decompose water into H₂ and O₂, which is considered to be one of the most green and efficient ways to produce hydrogen from water decomposition. Therefore, the coupling of oxidation reaction with hydrogen generation has become increasingly attractive. The thermodynamic and kinetic advantages of anodic oxidation over water oxidation result in a higher cathodic hydrogen yield. Current research in the field of PEC is mainly devoted to improving the efficiency of photoelectrolysis of water for hydrogen production by improving the performance of photoanodes, but it has not achieved the expected results. This section will set out the potential of SACs to enhance biomass photoelectrochemistry.

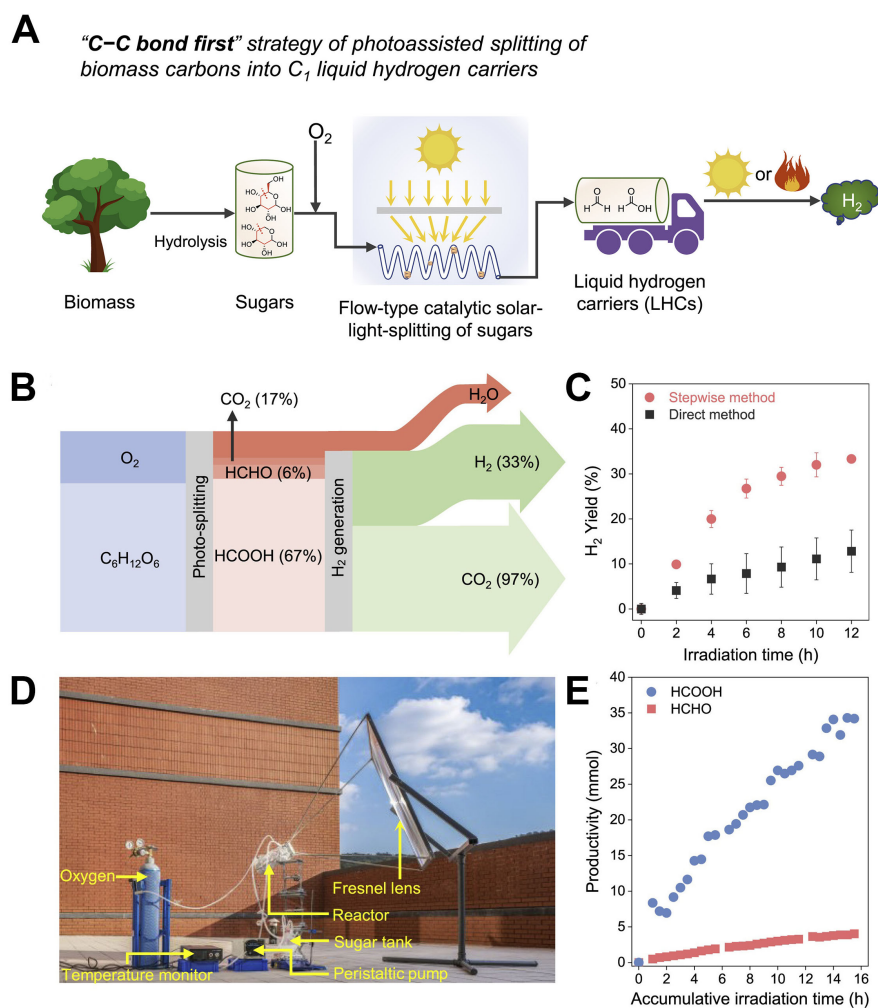


Figure 22. (A) Illustration of a stepwise method for H₂ production from biomass and storage in the form of C₁ LHCs; (B–D) Photocatalytic glucose decomposition to H₂ and CO₂ and solar-light driven glucose oxidation to C₁ LHCs; (E) Reaction results of flow-type glucose oxidation driven by concentrated solar light^[133]. Copyright 2023 Elsevier. LHCs: liquid hydrogen carriers.

Few studies have discussed the value conversion of glucose, and in this study, Tian *et al.* provide a good method to selectively oxidize glucose to high value glucosinolates. The use of defective TiO₂ as a photoanode, modulates the carrier current and improves charge separation, and the loading of Pt monoatoms onto the anode significantly improves the selectivity and yield of the C₆ product [Figure 23]. The final results show that the metal monoatom modified anode achieved a glucose oxidation photocurrent density of 1.91 mAcm⁻² at 0.6 V relative to the reversible hydrogen electrode, with a glucosonic acid yield of 84.3% under simulated sunlight irradiation^[135]. This work opens our eyes to the possibilities between PEC strategies and SACs, providing new inspiration for biomass catalysis from multiple perspectives.

A Pt single-atom dispersed WO₃ amorphous/crystalline homojunction for anodic glycerol oxidation reaction (GOR) coupled with cathodic hydrogen generation was recently reported by Feng *et al.*^[137]. Experimental data and DFT calculations have demonstrated that the isolated Pt single-atom and vacancies regulate the band structure, built-in electric field, and surface charge density. This promotes the transfer of holes from the bulk to the surface and accelerates the conversion of glycerol with a middle hydroxyl to carbon-centered radicals. The coupled photoelectrocatalytic system allows for the simultaneous anodic

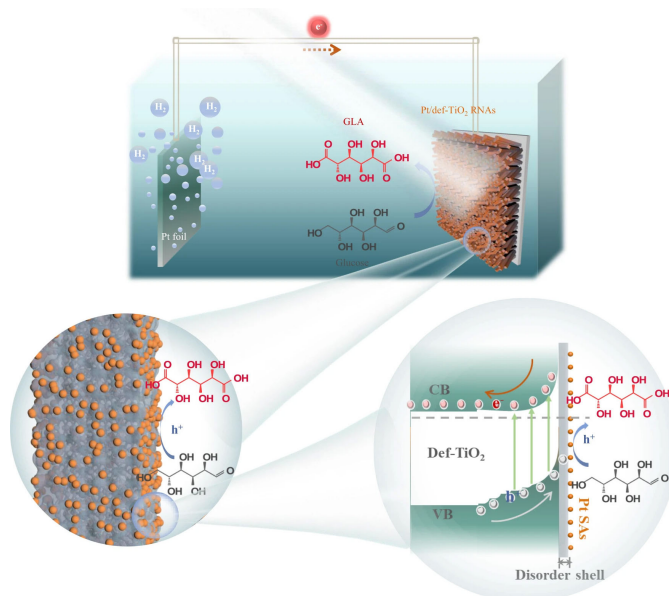


Figure 23. The schematic illustration of selective PEC oxidation of glucose to GLA over the single-atom Pt decorated defective TiO₂ photoanode^[135]. Copyright 2023 Springer Nature. PEC: Potoelectrochemical; GLA: glucosonic acid.

organic PEC conversion for high-value chemicals and cathodic hydrogen generation. The Pt-SA/WO_x photoanode exhibits superior PEC activity, achieving a photocurrent density of 2.85 mA cm⁻² at 1.2 V versus RHE. It also exhibits a glycerol conversion rate of up to 297.3 mmol m⁻² h⁻¹ and a DHA selectivity of 60.2%, while generating cathodic hydrogen at a rate of 203.2 mmol m⁻² h⁻¹.

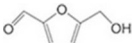


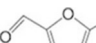

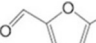




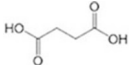
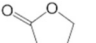
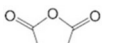
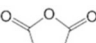
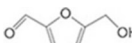
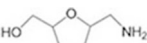
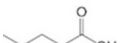
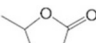




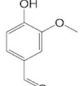
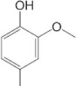
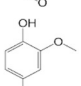
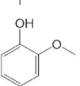
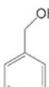
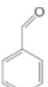


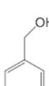
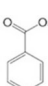
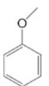
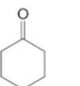
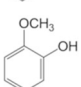
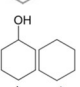
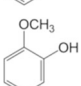
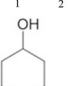
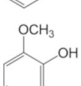
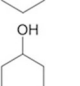
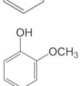
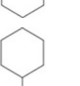
CONCLUSION AND OUTLOOK

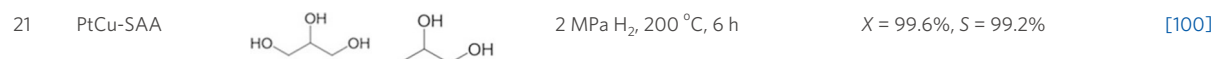
As mentioned above, SACs have emerged as a promising candidate for advancing biomass catalytic conversion including thermocatalysis, electrocatalysis, photocatalysis and photoelectrocatalysis. This catalytic approach offers various advantages, including reduced energy requirements, enhanced catalytic precision, and improved stability. Consequently, researchers worldwide have dedicated significant efforts and resources to the advancement of biorefinery technologies capable of processing diverse biomass feedstocks. In this review, we comprehensively summarized the impact of SACs across a broad field of biomass upgrading strategies encompassing diverse reaction types such as hydro(deoxy)genation^[42-45,48,51,52,57,63], oxidation^[46,47,72-74], RCF^[110-113] etc., as summarized in Table 1. The substrates investigated include a wide range of lignocellulosic feedstocks comprising furans, sugars, alcohols and polyols, ketones, acids and lignin derivatives. Despite showcasing promising efficacy in the realm of biomass conversion, it is evident that this catalytic technology is still in its nascent developmental stages. Therefore, the challenges and future developments may fall into the following categories.

From the perspective of biomass valorization

Typically, SACs focus on catalyzing the small molecule compounds produced in the downstream process. Compared with more structurally complex components such as lignin, only a few studies have dealt with its catalytic conversion. In contrast, SACs did not show particularly good catalytic advantages in the catalytic reduction fractionation of lignin. Since the metal loading of monoatomic catalysts is usually in the range of 0.1-5 wt%, more catalysts have to be used in the thermal catalysis of biomass. Moreover, the catalytic strategy developed for SACs did not achieve promising results than commercially available catalysts.

Table 1. Catalytic performance of some SACs in thermocatalytic reactions

Entry	Catalyst	Reactant	Product	Reaction conditions	Results	Ref.
1	Pt _v /Co (SAA)			1.0 MPa H ₂ , 180 °C, 2 h	X = 100%, S = 92.9%	[41]
2	Pt _v /Ni ₃ Fe			1.0 MPa H ₂ , 160 °C, 90 min	X = 99.0%, S = 98.1%	[42]
3	Pt _v /Nb ₂ O ₅ -Ov			4.0 MPa H ₂ , 160 °C, 1 h	S = 99% TOF = 2,553 h ⁻¹	[44]
4	(Co ₁ →Co _p)/N-CNTs			0.1 MPa H ₂ , 100 °C, 8 h	X = 100%, S = 96%	[46]
5	Mn-Co/N-C			0.6 MPa H ₂ , 80 °C, 8 h	Y = 95.8%	[47]
6	0.1Pd/γ-AlOOH			7 MPa H ₂ , 240 °C, 7 h	X = 73.5%, S = 98.7%, TOF = 305.4 h ⁻¹	[48]
7	Pt _v /1T-MoS ₂					[50]
8	Pd _v /BNC			0.5 MPa H ₂ , 0.2 MPa NH ₃ , 80 °C, 6 h	X = 100%, S = 96%	[49]
9	Ru ₁ @WO _x /CN			2 MPa H ₂ , 100 °C, 2 h Solvent-free	X = 99%, S = 100%	[51]
10	Ir _v /mpg-C ₃ N ₄			1 MPa H ₂ , 140 °C, 6 h	X = 99%, S = 100%	[60]
11	Fe-ZIF-8-800			120 °C, 1 h	X = 93.1%, S = 93.5%	[63]
12	Ru _v /mpg-C ₃ N ₄			4 MPa H ₂ , 140 °C, 4 h	X = 100%, S = 100%	[70]
				4 MPa H ₂ , 60 °C, 72 h	X = 95%, S = 100%	
13	Au@Pd/TiO ₂			O ₂ 50ml min ⁻¹ , 90 °C, 4 h, Solvent-free	X = 14.3%, S = 91.6%, TOF = 21,961 h ⁻¹	[72]
14	Au _v /CeO ₂			0.5 MPa O ₂ , 150 °C, 8 h, Solvent-free	X = 51.9%, S = 93%, TOF = 3283 h ⁻¹	[73]
15	Co SAs-N@C			0.1 MPa O ₂ , 60 °C, 3 h,	X = 99.8%, S = 97.5%	[74]
16	Pd _v /ZSM-5			2 MPa H ₂ , 180 °C, 3h, Water-solvent	S = 91.2%, TOR = 400.8 h ⁻¹	[75]
17	RuCo-300			1 MPa H ₂ , 250 °C, 2 h	X = 100%, S ₁ = 56.2% S ₂ = 31.3%	[81]
18	Ru/CeO ₂ -S			1 MPa H ₂ , 200 °C, 5h, Water-solvent	X = 99.9%, S = 99.9%	[82]
19	Co ₁ -NPs@NC			0.5 MPa H ₂ , 180 °C, 3 h	X = 100%, S = 97.1%	[83]
20	Ni _v /β-Mo ₂ C			4 MPa H ₂ , 260 °C, 4 h	X = 99.9%, S = 99.9%, TON = 1683 h ⁻¹	[84]



SAA: single-atom alloy; CNTs: carbon nanotubes; X: conversion; S: selectivity; SACs: single atom catalysts; TOF: turnover frequency.

Therefore, the efficient catalytic conversion of raw biomass material remains at the forefront of SACs research.

From the perspective of developing advanced catalytic systems

Although there have been increasing reports on advanced technologies for fabricating SACs, such as coordination pyrolysis, defect engineering, alloy dilution, impregnation, deposition precipitation (DP), atomic layer deposition (ALD), sol-gel, and ball milling, *etc.* Nevertheless, most of these strategies are developed at the laboratory scale and necessitate harsh and intricate operational conditions. In addition, when the metal particles are reduced to the single-atom level, the specific surface area increases dramatically, leading to a sharp increase in the free energy of the metal surface, which is highly susceptible to agglomeration coupling to form large clusters during preparation and reaction, thus leading to catalyst deactivation. In thermocatalysis, high-temperature environments may lead to a decrease in the stability of the SAC. Moreover, for the activation, breaking or generation of certain chemical bonds, a single metal atom may not provide the active site required for catalysis. Therefore, the current research trend has shifted from solely focusing on catalysis with single metal sites or alloys to embracing dual-site catalysis (single metal) to explore more catalytic possibilities. The presence of diverse metal active sites within SACs, including single-metal sites, bimetallic alloy sites or combinations of single-metal sites with NPs or nanoclusters (NCs), can lead to significant variations in catalytic performance. In consequence, future research will concentrate on the preparation of more stable and durable SACs and the development of tunable site configurations in SACs.

From the perspective of potential industrial applications

Despite the ongoing positive advancements in this field, practical applications in related industries have yet to be observed. Biomass feedstocks are inherently complex and often encounter a wide range of impurities and side reactions during practical implementation; this makes biomass conversion difficult in industrial applications. So, we need higher loading and higher activity SACs for industrial high productivity. Pretreatment of biomass feedstocks is harsh, such as high temperatures, high pressures, and polar and acidic media; the improvement of catalyst stability is also essential. Additionally, achieving mass production of SACs poses a significant challenge as only a limited number can currently be produced on a kilogram scale, and cost and equipment should also be considered. All results obtained thus far have been confined to laboratory settings without considering the multifactorial effects in production. In the face of these challenges, sustained research and innovation are needed to improve the efficiency, scalability and economy of SACs preparation and characterization technologies, and to strengthen industry-university-research collaboration to promote rapid technology translation and industrial application.

In conclusion, the aforementioned summary presents novel prospects and implications for the advancement of SAC and biomass conversion, offering extensive research opportunities. With advancements in detection technology and modern material science, SACs are poised to witness a surge in development opportunities. Furthermore, within the context of globalization, interdisciplinary integration will provide an enhanced innovative space for biomass and SACs.

DECLARATIONS

Authors' contributions

Made the literature review and drafted the original version: Gao, Y.; Cheng, J.

Revised the manuscript: Gao, Y.; Cheng, J.

Conceived and supervised the project: Sun, Z.; Liu, X.

Availability of data and materials

Not applicable.

Financial support and sponsorship

The authors thank the foundational support by the National Natural Science Foundation of China (22378024 and 22101029) and Beijing Municipal-Natural-Science Foundation (2222006).

Conflicts of interest

All authors declared that there are no conflicts of interest.

Ethical approval and consent to participate

Not applicable.

Consent for publication

Not applicable.

Copyright

© The Author(s) 2025.

REFERENCES

1. Upton, B. M.; Kasko, A. M. Strategies for the conversion of lignin to high-value polymeric materials: peview and perspective. *Chem. Rev.* **2016**, *116*, 2275-306. [DOI](#) [PubMed](#)
2. Zhang, Z.; Huber, G. W. Catalytic oxidation of carbohydrates into organic acids and furan chemicals. *Chem. Soc. Rev.* **2018**, *47*, 1351-90. [DOI](#) [PubMed](#)
3. Möller, M.; Schröder, U. Hydrothermal production of furfural from xylose and xylan as model compounds for hemicelluloses. *RSC. Adv.* **2013**, *3*, 22253. [DOI](#)
4. Liu, L.; Corma, A. Metal catalysts for heterogeneous catalysis: from single atoms to nanoclusters and nanoparticles. *Chem. Rev.* **2018**, *118*, 4981-5079. [DOI](#) [PubMed](#) [PMC](#)
5. Alonso, D. M.; Wettstein, S. G.; Dumesic, J. A. Bimetallic catalysts for upgrading of biomass to fuels and chemicals. *Chem. Soc. Rev.* **2012**, *41*, 8075-98. [DOI](#) [PubMed](#)
6. Deng, W.; Feng, Y.; Fu, J.; et al. Catalytic conversion of lignocellulosic biomass into chemicals and fuels. *Green. Energy. Environ.* **2023**, *8*, 10-114. [DOI](#)
7. Wyman, C. E.; Dale, B. E.; Elander, R. T.; Holtzapple, M.; Ladisch, M. R.; Lee, Y. Y. Coordinated development of leading biomass pretreatment technologies. *Bioresour. Technol.* **2005**, *96*, 1959-66. [DOI](#) [PubMed](#)
8. Klemm, D.; Heublein, B.; Fink, H. P.; Bohn, A. Cellulose: fascinating biopolymer and sustainable raw material. *Angew. Chem. Int. Ed. Engl.* **2005**, *44*, 3358-93. [DOI](#) [PubMed](#)
9. Huang, Y.; Fu, Y. Hydrolysis of cellulose to glucose by solid acid catalysts. *Green. Chem.* **2013**, *15*, 1095. [DOI](#)
10. Wu, X.; Luo, N.; Xie, S.; et al. Photocatalytic transformations of lignocellulosic biomass into chemicals. *Chem. Soc. Rev.* **2020**, *49*, 6198-223. [DOI](#)
11. Fang, R.; Dhakshinamoorthy, A.; Li, Y.; Garcia, H. Metal organic frameworks for biomass conversion. *Chem. Soc. Rev.* **2020**, *49*, 3638-87. [DOI](#) [PubMed](#)
12. Bozell, J. J.; Petersen, G. R. Technology development for the production of biobased products from biorefinery carbohydrates-the US Department of Energy's "Top 10" revisited. *Green. Chem.* **2010**, *12*, 539. [DOI](#)
13. Motagamwala, A. H.; Huang, K.; Maravelias, C. T.; Dumesic, J. A. Solvent system for effective near-term production of hydroxymethylfurfural (HMF) with potential for long-term process improvement. *Energy. Environ. Sci.* **2019**, *12*, 2212-22. [DOI](#)
14. Liu, X.; Duan, X.; Wei, W.; Wang, S.; Ni, B. Photocatalytic conversion of lignocellulosic biomass to valuable products. *Green. Chem.* **2019**, *21*, 4266-89. [DOI](#)

15. Mondelli, C.; Gözaydın, G.; Yan, N.; Pérez-Ramírez, J. Biomass valorisation over metal-based solid catalysts from nanoparticles to single atoms. *Chem. Soc. Rev.* **2020**, *49*, 3764-82. DOI PubMed
16. Abreu, T. C.; Ciotonea, C.; Le, V. A.; et al. Optimization of catalyst activity and stability in the m-cresol hydrodeoxygenation through Ni particle size control. *Appl. Catal. B. Environ.* **2023**, *338*, 123030. DOI
17. Lim, K. R. G.; Kaiser, S. K.; Wu, H.; et al. Nanoparticle proximity controls selectivity in benzaldehyde hydrogenation. *Nat. Catal.* **2024**, *7*, 172-84. DOI
18. Qiao, B.; Wang, A.; Yang, X.; et al. Single-atom catalysis of CO oxidation using Pt₁/FeO_x. *Nat. Chem.* **2011**, *3*, 634-41. DOI
19. Liu, D.; He, Q.; Ding, S.; Song, L. Structural regulation and support coupling effect of single-atom catalysts for heterogeneous catalysis. *Adv. Energy. Mater.* **2020**, *10*, 2001482. DOI
20. Zhou, X.; Shen, Q.; Yuan, K.; et al. Unraveling charge state of supported Au single-atoms during CO oxidation. *J. Am. Chem. Soc.* **2018**, *140*, 554-7. DOI
21. Xue, J.; Dong, X.; Liu, C.; et al. Turning copper into an efficient and stable CO evolution catalyst beyond noble metals. *Nat. Commun.* **2024**, *15*, 5998. DOI PubMed PMC
22. Zhang, F.; Zhu, Y.; Lin, Q.; Zhang, L.; Zhang, X.; Wang, H. Noble-metal single-atoms in thermocatalysis, electrocatalysis, and photocatalysis. *Energy. Environ. Sci.* **2021**, *14*, 2954-3009. DOI
23. Zhang, L.; Ren, Y.; Liu, W.; Wang, A.; Zhang, T. Single-atom catalyst: a rising star for green synthesis of fine chemicals. *Natl. Sci. Rev.* **2018**, *5*, 653-72. DOI
24. Lu, Y.; Zhang, Z.; Wang, H.; Wang, Y. Toward efficient single-atom catalysts for renewable fuels and chemicals production from biomass and CO₂. *Appl. Catal. B. Environ.* **2021**, *292*, 120162. DOI
25. Zhu, C.; Fu, S.; Shi, Q.; Du, D.; Lin, Y. Single-atom electrocatalysts. *Angew. Chem. Int. Ed. Engl.* **2017**, *56*, 13944-60. DOI PubMed
26. Su, J.; Ge, R.; Dong, Y.; Hao, F.; Chen, L. Recent progress in single-atom electrocatalysts: concept, synthesis, and applications in clean energy conversion. *J. Mater. Chem. A.* **2018**, *6*, 14025-42. DOI
27. Wang, Y.; Su, H.; He, Y.; et al. Advanced electrocatalysts with single-metal-atom active sites. *Chem. Rev.* **2020**, *120*, 12217-314. DOI
28. Gao, C.; Low, J.; Long, R.; Kong, T.; Zhu, J.; Xiong, Y. Heterogeneous single-atom photocatalysts: fundamentals and applications. *Chem. Rev.* **2020**, *120*, 12175-216. DOI
29. Chen, C.; Li, J.; Tan, X.; et al. Harnessing single-atom catalysts for CO₂ electroreduction: a review of recent advances. *EES. Catal.* **2024**, *2*, 71-93. DOI
30. Wang, H.; Tong, Y.; Chen, P. Microenvironment regulation strategies of single-atom catalysts for advanced electrocatalytic CO₂ reduction to CO. *Nano. Energy.* **2023**, *118*, 108967. DOI
31. Yuan, W.; Ma, Y.; Wu, H.; Cheng, L. Single-atom catalysts for CO oxidation, CO₂ reduction, and O₂ electrochemistry. *J. Energy. Chem.* **2022**, *69*, 347. DOI
32. Sun, Q.; Jia, C.; Zhao, Y.; Zhao, C. Single atom-based catalysts for electrochemical CO₂ reduction. *Chinese. J. Catal.* **2022**, *43*, 1547-97. DOI
33. Li, L.; Huang, B.; Tang, X.; et al. Recent developments of microenvironment engineering of single-atom catalysts for oxygen reduction toward desired activity and selectivity. *Adv. Funct. Mater.* **2021**, *31*, 2103857. DOI
34. Yan, L.; Li, P.; Zhu, Q.; et al. Atomically precise electrocatalysts for oxygen reduction reaction. *Chem* **2023**, *9*, 280-342. DOI
35. Jiang, F.; Li, Y.; Pan, Y. Design principles of single-atom catalysts for oxygen evolution reaction: from targeted structures to active sites. *Adv. Mater.* **2024**, *36*, e2306309. DOI
36. Iqbal, S.; Safdar, B.; Hussain, I.; Zhang, K.; Chatzichristodoulou, C. Trends and prospects of bulk and single-atom catalysts for the oxygen evolution reaction. *Adv. Energy. Mater.* **2023**, *13*, 2203913. DOI
37. De, S.; Burange, A. S.; Luque, R. Conversion of biomass-derived feedstocks into value-added chemicals over single-atom catalysts. *Green. Chem.* **2022**, *24*, 2267-86. DOI
38. Chen, J.; Xiao, Y.; Guo, F.; Li, K.; Huang, Y.; Lu, Q. Single-atom metal catalysts for catalytic chemical conversion of biomass to chemicals and fuels. *ACS. Catal.* **2024**, *14*, 5198-226. DOI
39. Tian, X.; Wang, Y.; Zeng, Z.; et al. Research progress on the role of common metal catalysts in biomass pyrolysis: a state-of-the-art review. *Green. Chem.* **2022**, *24*, 3922-42. DOI
40. Yang, P.; Xia, Q.; Liu, X.; Wang, Y. Catalytic transfer hydrogenation/hydrogenolysis of 5-hydroxymethylfurfural to 2,5-dimethylfuran over Ni-Co/C catalyst. *Fuel* **2017**, *187*, 159-66. DOI
41. Wang, X.; Liu, Y.; Liang, X. Hydrogenolysis of 5-hydroxymethylfurfural to 2,5-dimethylfuran over supported Pt-Co bimetallic catalysts under mild conditions. *Green. Chem.* **2018**, *20*, 2894-902. DOI
42. Gan, T.; Liu, Y.; He, Q.; Zhang, H.; He, X.; Ji, H. Facile synthesis of kilogram-scale Co-alloyed Pt single-atom catalysts via ball milling for hydrodeoxygenation of 5-hydroxymethylfurfural. *ACS. Sustainable. Chem. Eng.* **2020**, *8*, 8692-9. DOI
43. Meng, G.; Ji, K.; Zhang, W.; et al. Tandem catalyzing the hydrodeoxygenation of 5-hydroxymethylfurfural over a Ni₃Fe intermetallic supported Pt single-atom site catalyst. *Chem. Sci.* **2021**, *12*, 4139-46. DOI
44. Wang, L.; Yang, Y.; Shi, Y.; et al. Single-atom catalysts with metal-acid synergistic effect toward hydrodeoxygenation tandem reactions. *Chem. Catal.* **2023**, *3*, 100483. DOI
45. Li, S.; Dong, M.; Yang, J.; et al. Selective hydrogenation of 5-(hydroxymethyl)furfural to 5-methylfurfural over single atomic metals

- anchored on Nb₂O₅. *Nat. Commun.* **2021**, *12*, 584. DOI PubMed PMC
46. Yang, S.; Wu, C.; Wang, J.; et al. Metal single-atom and nanoparticle double-active-site relay catalysts: design, preparation, and application to the oxidation of 5-hydroxymethylfurfural. *ACS. Catal.* **2022**, *12*, 971-81. DOI
 47. Zhang, M.; Ma, H.; Liu, X.; et al. Control in local coordination environment boosting activating molecular oxygen with an atomically dispersed binary Mn-Co catalyst. *ACS. Appl. Mater. Interfaces.* **2022**, *14*, 18539-49. DOI
 48. Zhang, C.; Chen, L.; Cheng, H.; Zhu, X.; Qi, Z. Atomically dispersed Pd catalysts for the selective hydrogenation of succinic acid to γ -butyrolactone. *Catal. Today.* **2016**, *276*, 55-61. DOI
 49. Liu, W. J.; Zhou, X.; Min, Y.; et al. Engineering of local coordination microenvironment in single-atom catalysts enabling sustainable conversion of biomass into a broad range of amines. *Adv. Mater.* **2024**, *36*, e2305924. DOI
 50. Sun, X.; Zhao, Y.; Chang, K.; et al. 1T-phase MoS₂ edge-anchored Pt₁-S₃ active site boosting selective hydrogenation of biomass-derived maleic anhydride. *Rare. Met.* **2023**, *42*, 2658-69. DOI
 51. Han, Y.; Dai, J.; Xu, R.; et al. Notched-polyoxometalate strategy to fabricate atomically dispersed Ru catalysts for biomass conversion. *ACS. Catal.* **2021**, *11*, 2669-75. DOI
 52. Shao, S.; Yang, Y.; Sun, K.; et al. Electron-rich ruthenium single-atom alloy for aqueous levulinic acid hydrogenation. *ACS. Catal.* **2021**, *11*, 12146-58. DOI
 53. Gao, J.; Feng, L.; Ma, R.; et al. Cobalt single-atom catalysts for domino reductive amination and amidation of levulinic acid and related molecules to N-heterocycles. *Chem. Catal.* **2022**, *2*, 178-94. DOI
 54. Ji, N.; Zhang, T.; Zheng, M.; et al. Direct catalytic conversion of cellulose into ethylene glycol using nickel-promoted tungsten carbide catalysts. *Angew. Chem. Int. Ed. Engl.* **2008**, *47*, 8510-3. DOI
 55. Yang, C.; Miao, Z.; Zhang, F.; et al. Hydrogenolysis of methyl glycolate to ethanol over a Pt-Cu/SiO₂ single-atom alloy catalyst: a further step from cellulose to ethanol. *Green. Chem.* **2018**, *20*, 2142-50. DOI
 56. Liu, W.; Chen, Y.; Qi, H.; et al. A durable nickel single-atom catalyst for hydrogenation reactions and cellulose valorization under harsh conditions. *Angew. Chem. Int. Ed. Engl.* **2018**, *57*, 7071-5. DOI
 57. Zhang, L.; Meng, G.; Zhang, W.; et al. Oriented conversion of a LA/HMF mixture to GVL and FDCA in a biphasic solvent over a Ru single-atom/nanoparticle dual-site catalyst. *ACS. Catal.* **2023**, *13*, 2268-76. DOI
 58. Fu, J.; Lym, J.; Zheng, W.; et al. C-O bond activation using ultralow loading of noble metal catalysts on moderately reducible oxides. *Nat. Catal.* **2020**, *3*, 446-53. DOI
 59. Ishida, T.; Honma, T.; Nakada, K.; et al. Pd-catalyzed decarbonylation of furfural: elucidation of support effect on Pd size and catalytic activity using in-situ XAFS. *J. Catal.* **2019**, *374*, 320-7. DOI
 60. Tian, S.; Gong, W.; Chen, W.; et al. Regulating the catalytic performance of single-atomic-site Ir catalyst for biomass conversion by metal-support interactions. *ACS. Catal.* **2019**, *9*, 5223-30. DOI
 61. Zhu, Y.; Zhao, W.; Zhang, J.; et al. Selective activation of C-OH, C-O-C, or C=C in furfuryl alcohol by engineered Pt sites supported on layered double oxides. *ACS. Catal.* **2020**, *10*, 8032-41. DOI
 62. Qi, H.; Li, Y.; Zhou, Z.; et al. Synthesis of piperidines and pyridine from furfural over a surface single-atom alloy Ru₁Co_{NP} catalyst. *Nat. Commun.* **2023**, *14*, 6329. DOI PubMed PMC
 63. An, Z.; Yang, P.; Duan, D.; et al. Highly active, ultra-low loading single-atom iron catalysts for catalytic transfer hydrogenation. *Nat. Commun.* **2023**, *14*, 6666. DOI PubMed PMC
 64. Chen, X.; Guan, W.; Tsang, C.; Hu, H.; Liang, C. Lignin valorizations with Ni catalysts for renewable chemicals and fuels productions. *Catal* **2019**, *9*, 488. DOI
 65. Rinaldi, R.; Jastrzebski, R.; Clough, M. T.; et al. Paving the way for lignin valorisation: recent advances in bioengineering, biorefining and catalysis. *Angew. Chem. Int. Ed. Engl.* **2016**, *55*, 8164-215. DOI PubMed PMC
 66. Chen, X.; Zhang, B.; Wang, Y.; Yan, N. Valorization of renewable carbon resources for chemicals. *Chimia* **2015**, *69*, 120-4. DOI
 67. Dong, L.; Xin, Y.; Liu, X.; et al. Selective hydrodeoxygenation of lignin oil to valuable phenolics over Au/Nb₂O₅ in water. *Green. Chem.* **2019**, *21*, 3081-90. DOI
 68. Horáček, J.; Šťábová, G.; Kelbichová, V.; Kubička, D. Zeolite-beta-supported platinum catalysts for hydrogenation/hydrodeoxygenation of pyrolysis oil model compounds. *Catal. Today.* **2013**, *204*, 38-45. DOI
 69. Yan, K.; Wang, D.; Li, H. Atom doping engineering of metal/carbon catalysts for biomass hydrodeoxygenation. *ACS. Sustainable. Chem. Eng.* **2021**, *9*, 16531-55. DOI
 70. Tian, S.; Wang, Z.; Gong, W.; et al. Temperature-controlled selectivity of hydrogenation and hydrodeoxygenation in the conversion of biomass molecule by the Ru₁/mpg-C₃N₄ catalyst. *J. Am. Chem. Soc.* **2018**, *140*, 11161-4. DOI
 71. Li, Z.; Lu, X.; Sun, W.; et al. One-step synthesis of single palladium atoms in WO_{2.72} with high efficiency in chemoselective hydrodeoxygenation of vanillin. *Appl. Catal. B: Environ.* **2021**, *298*, 120535. DOI
 72. Sun, J.; Han, Y.; Fu, H.; Qu, X.; Xu, Z.; Zheng, S. Au@Pd/TiO₂ with atomically dispersed Pd as highly active catalyst for solvent-free aerobic oxidation of benzyl alcohol. *Chem. Eng. J.* **2017**, *313*, 1-9. DOI
 73. Li, T.; Liu, F.; Tang, Y.; et al. Maximizing the number of interfacial sites in single-atom catalysts for the highly selective, solvent-free oxidation of primary alcohols. *Angew. Chem. Int. Ed. Engl.* **2018**, *57*, 7795-9. DOI
 74. Zhou, H.; Hong, S.; Zhang, H.; et al. Toward biomass-based single-atom catalysts and plastics: highly active single-atom Co on N-doped carbon for oxidative esterification of primary alcohols. *Appl. Catal. B. Environ.* **2019**, *256*, 117767. DOI
 75. Xu, K.; Chen, Y.; Yang, H.; et al. Partial hydrogenation of anisole to cyclohexanone in water medium catalyzed by atomically

- dispersed Pd anchored in the micropores of zeolite. *Appl. Catal. B. Environ.* **2024**, *341*, 123244. DOI
76. Liu, S.; Bai, L.; van, M. A. P.; et al. Oxidative cleavage of β -O-4 bonds in lignin model compounds with a single-atom Co catalyst. *Green. Chem.* **2019**, *21*, 1974-81. DOI
77. Kusumoto, S.; Nozaki, K. Direct and selective hydrogenolysis of arenols and aryl methyl ethers. *Nat. Commun.* **2015**, *6*, 6296. DOI PubMed
78. Prasomsri, T.; Shetty, M.; Murugappan, K.; Román-leshkov, Y. Insights into the catalytic activity and surface modification of MoO₃ during the hydrodeoxygenation of lignin-derived model compounds into aromatic hydrocarbons under low hydrogen pressures. *Energy. Environ. Sci.* **2014**, *7*, 2660-9. DOI
79. Olcese, R.; Bettahar, M.; Malaman, B.; et al. Gas-phase hydrodeoxygenation of guaiacol over iron-based catalysts. Effect of gases composition, iron load and supports (silica and activated carbon). *Appl. Catal. B. Environ.* **2013**, *129*, 528-38. DOI
80. Li, C.; Nakagawa, Y.; Yabushita, M.; Nakayama, A.; Tomishige, K. Guaiacol hydrodeoxygenation over iron-ceria catalysts with platinum single-atom alloy clusters as a promoter. *ACS. Catal.* **2021**, *11*, 12794-814. DOI
81. Xiang, L.; Fan, G.; Yang, L.; Zheng, L.; Li, F. Structure-tunable pompon-like RuCo catalysts: insight into the roles of atomically dispersed Ru-Co sites and crystallographic structures for guaiacol hydrodeoxygenation. *J. Catal.* **2021**, *398*, 76-88. DOI
82. Wang, B.; Zhou, P.; Yan, X.; Li, H.; Wu, H.; Zhang, Z. Cooperative catalysis of Co single atoms and nanoparticles enables selective C_{Ar}-OCH₃ cleavage for sustainable production of lignin-based cyclohexanols. *J. Energy. Chem.* **2023**, *79*, 535-49. DOI
83. Guo, H.; Zhao, J.; Chen, Y.; et al. Mechanistic insights into hydrodeoxygenation of lignin derivatives over Ni single atoms supported on Mo₂C. *ACS. Catal.* **2024**, *14*, 703-17. DOI
84. Zhang, K.; Meng, Q.; Wu, H.; et al. Selective hydrodeoxygenation of aromatics to cyclohexanols over Ru single atoms supported on CeO₂. *J. Am. Chem. Soc.* **2022**, *144*, 20834-46. DOI
85. Chen, L.; Pan, L.; van, M. A. P.; et al. Anchoring single platinum atoms onto nickel nanoparticles affords highly selective catalysts for lignin conversion. *Cell. Rep. Phys. Sci.* **2021**, *2*, 100567. DOI
86. Meng, G.; Lan, W.; Zhang, L.; et al. Synergy of single atoms and lewis acid sites for efficient and selective lignin disassembly into monolignol derivatives. *J. Am. Chem. Soc.* **2023**, *145*, 12884-93. DOI
87. Tobimatsu, Y.; Chen, F.; Nakashima, J.; et al. Coexistence but independent biosynthesis of catechyl and guaiacyl/syringyl lignin polymers in seed coats. *Plant. Cell.* **2013**, *25*, 2587-600. DOI PubMed PMC
88. Zhuo, C.; Rao, X.; Azad, R.; et al. Enzymatic basis for C-lignin monomer biosynthesis in the seed coat of cleome hassleriana. *Plant. J.* **2019**, *99*, 506-20. DOI
89. Wang, S.; Zhang, K.; Li, H.; Xiao, L. P.; Song, G. Selective hydrogenolysis of catechyl lignin into propenylcatechol over an atomically dispersed ruthenium catalyst. *Nat. Commun.* **2021**, *12*, 416. DOI PubMed PMC
90. Jiang, M.; Chen, X.; Wang, L.; Liang, J.; Wei, X.; Nong, W. Anchoring single Ni atoms on CeO₂ nanospheres as an efficient catalyst for the hydrogenolysis of lignin to aromatic monomers. *Fuel* **2022**, *324*, 124499. DOI
91. Liu, C. X.; Liu, K.; Xu, Y.; et al. Photocatalytic upgrading of polylactic acid waste into alanine under mild conditions. *Angew. Chem. Int. Ed. Engl.* **2024**, *63*, e202401255. DOI
92. Taarning, E.; Madsen, A. T.; Marchetti, J. M.; Egeblad, K.; Christensen, C. H. Oxidation of glycerol and propanediols in methanol over heterogeneous gold catalysts. *Green. Chem.* **2008**, *10*, 408. DOI
93. Li, S.; Deng, W.; Li, Y.; Zhang, Q.; Wang, Y. Catalytic conversion of cellulose-based biomass and glycerol to lactic acid. *J. Energy. Chem.* **2019**, *32*, 138-51. DOI
94. Wang, S.; Yin, K.; Zhang, Y.; Liu, H. Glycerol hydrogenolysis to propylene glycol and ethylene glycol on zirconia supported noble metal catalysts. *ACS. Catal.* **2013**, *3*, 2112-21. DOI
95. Nakagawa, Y.; Tomishige, K. Heterogeneous catalysis of the glycerol hydrogenolysis. *Catal. Sci. Technol.* **2011**, *1*, 179. DOI
96. Renders, T.; Van, B. S.; Koelewijn, S.; Schutyser, W.; Sels, B. F. Lignin-first biomass fractionation: the advent of active stabilisation strategies. *Energy. Environ. Sci.* **2017**, *10*, 1551-7. DOI
97. Van, B. S.; Schutyser, W.; Vanholme, R.; et al. Reductive lignocellulose fractionation into soluble lignin-derived phenolic monomers and dimers and processable carbohydrate pulps. *Energy. Environ. Sci.* **2015**, *8*, 1748-63. DOI
98. Renders, T.; Cooreman, E.; Van, B. S.; et al. Catalytic lignocellulose biorefining in *n*-butanol/water: a one-pot approach toward phenolics, polyols, and cellulose. *Green. Chem.* **2018**, *20*, 4607-19. DOI
99. Wang, J.; Zhao, X.; Lei, N.; et al. Hydrogenolysis of glycerol to 1,3-propanediol under low hydrogen pressure over WO_x-supported single/pseudo-single atom Pt catalyst. *ChemSusChem* **2016**, *9*, 784-90. DOI
100. Zhang, X.; Cui, G.; Feng, H.; et al. Platinum-copper single atom alloy catalysts with high performance towards glycerol hydrogenolysis. *Nat. Commun.* **2019**, *10*, 5812. DOI
101. An, Z.; Zhang, Z.; Huang, Z.; et al. Pt₁ enhanced C-H activation synergistic with Pt_n catalysis for glycerol cascade oxidation to glyceric acid. *Nat. Commun.* **2022**, *13*, 5467. DOI PubMed PMC
102. Lou, Y.; Zheng, Y.; Li, X.; et al. Pocketlike active site of Rh₁/MoS₂ single-atom catalyst for selective crotonaldehyde hydrogenation. *J. Am. Chem. Soc.* **2019**, *141*, 19289-95. DOI
103. Lou, Y.; Zhao, Y.; Liu, H.; et al. Edge-confined Pt₁/MoS₂ single-atom catalyst promoting the selective activation of carbon-oxygen bond. *ChemCatChem* **2021**, *13*, 2783-93. DOI
104. Li, Z.; Dong, X.; Zhang, M.; et al. Selective hydrogenation on a highly active single-atom catalyst of palladium dispersed on ceria nanorods by defect engineering. *ACS. Appl. Mater. Interfaces.* **2020**, *12*, 57569-77. DOI

105. Li, Z.; Fan, T.; Li, H.; et al. Atomically defined undercoordinated copper active sites over nitrogen-doped carbon for aerobic oxidation of alcohols. *Small* **2022**, *18*, e2106614. DOI
106. Li, Z.; Leng, L.; Lu, X.; et al. Single palladium atoms stabilized by β -FeOOH nanorod with superior performance for selective hydrogenation of cinnamaldehyde. *Nano. Res.* **2022**, *15*, 3114-21. DOI
107. Li, Z.; Wei, W.; Li, H.; et al. Low-temperature synthesis of single palladium atoms supported on defective hexagonal boron nitride nanosheet for chemoselective hydrogenation of cinnamaldehyde. *ACS. Nano.* **2021**, *15*, 10175-84. DOI
108. Liang, Y.; Tang, Q.; Liu, L.; Wang, D.; Dong, J. Fabrication of highly oxidized Pt single-atom catalysts to suppress the deep hydrogenation of unsaturated aldehydes. *Appl. Catal. B. Environ.* **2023**, *333*, 122783. DOI
109. Li, X.; Liu, J.; Wu, J.; Zhang, L.; Cao, D.; Cheng, D. Constructing a highly active Pd atomically dispersed catalyst for cinnamaldehyde hydrogenation: synergistic catalysis between Pd-N₃ single atoms and fully exposed Pd clusters. *ACS. Catal.* **2024**, *14*, 2369-79. DOI
110. Park, J.; Cahyadi, H. S.; Mushtaq, U.; et al. Highly efficient reductive catalytic fractionation of lignocellulosic biomass over extremely low-loaded Pd catalysts. *ACS. Catal.* **2020**, *10*, 12487-506. DOI
111. Liu, Z.; Li, H.; Gao, X.; et al. Rational highly dispersed ruthenium for reductive catalytic fractionation of lignocellulose. *Nat. Commun.* **2022**, *13*, 4716. DOI PubMed PMC
112. Ge, J.; Wang, G.; Sui, W.; et al. Highly efficient metal-acid synergetic catalytic fractionation of lignocellulose under mild conditions over lignin-coordinated N-anchoring Co single-atom catalyst. *Chem. Eng. J.* **2023**, *462*, 142109. DOI
113. Miao, J.; Ma, Y.; Wang, X.; et al. Efficiently selective C(O-)-C bond cleavage for full lignocellulose upgrading coupled with energy-saving hydrogen production by Ir single-atom electrocatalyst. *Appl. Catal. B. Environ.* **2023**, *336*, 122937. DOI
114. Zhu, P.; Shi, M.; Shen, Z.; Liao, X.; Chen, Y. Electrocatalytic conversion of biomass-derived furan compounds: mechanisms, catalysts and perspectives. *Chem. Sci.* **2024**, *15*, 4723-56. DOI PubMed PMC
115. Yang, M.; Yuan, Z.; Peng, R.; Wang, S.; Zou, Y. Recent progress on electrocatalytic valorization of biomass-derived organics. *Energy. Environ. Mater.* **2022**, *5*, 1117-38. DOI
116. Ye, F.; Zhang, S.; Cheng, Q.; et al. The role of oxygen-vacancy in bifunctional indium oxyhydroxide catalysts for electrochemical coupling of biomass valorization with CO₂ conversion. *Nat. Commun.* **2023**, *14*, 2040. DOI PubMed PMC
117. Liu, S.; Gao, M.; Wu, S.; et al. A coupled electrocatalytic system with reduced energy input for CO₂ reduction and biomass valorization. *Energy. Environ. Sci.* **2023**, *16*, 5305-14. DOI
118. Zeng, L.; Chen, Y.; Sun, M.; et al. Cooperative Rh-O₃/Ni(Fe) site for efficient biomass upgrading coupled with H₂ production. *J. Am. Chem. Soc.* **2023**, *145*, 17577-87. DOI
119. Xu, C.; Paone, E.; Rodríguez-Padrón, D.; Luque, R.; Mauriello, F. Recent catalytic routes for the preparation and the upgrading of biomass derived furfural and 5-hydroxymethylfurfural. *Chem. Soc. Rev.* **2020**, *49*, 4273-306. DOI PubMed
120. Ji, K.; Xu, M.; Xu, S. M.; et al. Electrocatalytic hydrogenation of 5-hydroxymethylfurfural promoted by a Ru₁Cu single-atom alloy catalyst. *Angew. Chem. Int. Ed. Engl.* **2022**, *61*, e202209849. DOI
121. Lu, Y.; Liu, T.; Dong, C. L.; et al. Tuning the selective adsorption site of biomass on Co₃O₄ by Ir single atoms for electrosynthesis. *Adv. Mater.* **2021**, *33*, e2007056. DOI
122. Ge, R.; Wang, Y.; Li, Z.; et al. Selective electrooxidation of biomass-derived alcohols to aldehydes in a neutral medium: promoted water dissociation over a nickel-oxide-supported ruthenium single-atom catalyst. *Angew. Chem. Int. Ed. Engl.* **2022**, *61*, e202200211. DOI
123. Zhou, Y.; Slater, T. J.; Luo, X.; Shen, Y. A versatile single-copper-atom electrocatalyst for biomass valorization. *Appl. Catal. B. Environ.* **2023**, *324*, 122218. DOI
124. Mukadam, Z.; Liu, S.; Pedersen, A.; et al. Furfural electrovalorisation using single-atom molecular catalysts. *Energy. Environ. Sci.* **2023**, *16*, 2934-44. DOI
125. Qin, M.; Fan, S.; Li, X.; Tade, M. O.; Liu, S. Electroreductive CO coupling of benzaldehyde over SACs Au-NiMn₂O₄ spinel synergetic composites. *J. Colloid. Inter. Sci.* **2022**, *625*, 305-16. DOI
126. Wang, Y.; Zhu, Y. Q.; Xie, Z.; et al. Efficient electrocatalytic oxidation of glycerol via promoted OH* generation over single-atom-bismuth-doped spinel Co₃O₄. *ACS. Catal.* **2022**, *12*, 12432-43. DOI
127. Cui, T.; Ma, L.; Wang, S.; et al. Atomically dispersed Pt-N₃C₁ sites enabling efficient and selective electrocatalytic C-C bond cleavage in lignin models under ambient conditions. *J. Am. Chem. Soc.* **2021**, *143*, 9429-39. DOI
128. Yang, F.; Liu, S.; Tang, T.; Yao, S.; An, C. Visible-light driven H₂ evolution coupled with furfuryl alcohol selective oxidation over Ru atom decorated Zn_{0.5}Cd_{0.5}S nanorods. *Catal. Sci. Technol.* **2023**, *13*, 2469-74. DOI
129. Lu, X.; Guo, C.; Zhang, M.; et al. Rational design of palladium single-atoms and clusters supported on silicoaluminophosphate-31 by a photochemical route for chemoselective hydrodeoxygenation of vanillin. *Nano. Res.* **2021**, *14*, 4347-55. DOI
130. Deng, J.; Zhou, C.; Yang, Y.; et al. Visible-light-driven selective cleavage of CC bonds in lignin model substrates using carbon nitride-supported ruthenium single-atom catalyst. *Chem. Eng. J.* **2023**, *462*, 142282. DOI
131. Xiong, L.; Qi, H.; Zhang, S.; et al. Highly selective transformation of biomass derivatives to valuable chemicals by single-atom photocatalyst Ni/TiO₂. *Adv. Mater.* **2023**, *35*, e2209646. DOI
132. Xiong, L.; Yu, Z.; Cao, H.; Guan, W.; Su, Y.; et al. Converting glycerol into valuable trioses by Cu^{δ+}-single-atom-decorated WO₃ under visible light. *Angew. Chem. Int. Ed. Engl.* **2024**, *63*, e202318461. DOI
133. Ren, P.; Gao, Z.; Montini, T.; et al. Stepwise photoassisted decomposition of carbohydrates to H₂. *Joule* **2023**, *7*, 333-49. DOI

134. Li, W.; Zheng, X.; Xu, B. B.; et al. Atomic ruthenium-promoted cadmium sulfide for photocatalytic production of amino acids from biomass derivatives. *Angew. Chem. Int. Ed. Engl.* **2024**, *63*, e202320014. DOI
135. Tian, Z.; Da, Y.; Wang, M.; et al. Selective photoelectrochemical oxidation of glucose to glucaric acid by single atom Pt decorated defective TiO₂. *Nat. Commun.* **2023**, *14*, 142. DOI PubMed PMC
136. Lu, X.; Xie, S.; Yang, H.; Tong, Y.; Ji, H. Photoelectrochemical hydrogen production from biomass derivatives and water. *Chem. Soc. Rev.* **2014**, *43*, 7581-93. DOI
137. Feng, X.; Sun, T.; Feng, X.; et al. Single-atomic-site platinum steers middle hydroxyl selective oxidation on amorphous/crystalline homojunction for photoelectrochemical glycerol oxidation coupled with hydrogen generation. *Adv. Funct. Mater.* **2024**, *34*, 2316238. DOI